

Portland State University

PDXScholar

Dissertations and Theses

Dissertations and Theses

6-1-1968

Search for quantum oscillations in field emission current from bismuth.

Donald Dean Casey
Portland State University

Follow this and additional works at: https://pdxscholar.library.pdx.edu/open_access_etds

Let us know how access to this document benefits you.

Recommended Citation

Casey, Donald Dean, "Search for quantum oscillations in field emission current from bismuth." (1968). *Dissertations and Theses*. Paper 575.
<https://doi.org/10.15760/etd.575>

This Thesis is brought to you for free and open access. It has been accepted for inclusion in Dissertations and Theses by an authorized administrator of PDXScholar. Please contact us if we can make this document more accessible: pdxscholar@pdx.edu.

AN ABSTRACT OF THE THESIS OF

----- Donald Dean Casey ----- for the Master of Science -----
(Name of Student) (Degree)

in ----- Physics ----- presented on April 29, 1968 -----
(Major) (Date)

Title: Search for Quantum Oscillations in Field Emission Current -----

----- from Bismuth -----

Abstract approved: -----

(Signature)

Laird C. Brodie

An experimental search, based on previous published theoretical work, was made for de Haas-van Alphen-like quantum oscillations in field emission current. The study was motivated by the possible applicability of de Haas-van Alphen measurements to the study of Fermi surfaces near real surfaces.

Field emitters were fabricated from bismuth single crystals grown from the melt by a modified Bridgeman technique. Field emission current was measured with the field emitter cooled by contact with a liquid helium bath. Most measurements were made at 4.2°K, although a few measurements were made at 2.02°K. Fowler-Nordheim plots of the experimental current-voltage data were linear over several orders of magnitude. The field emission current was measured as a function of

magnetic field strength to twenty kilogauss and as a function of direction, with respect to the emitter axis, for a steady field of ten kilogauss. The results of measurements on four field emitter crystals are reported in this thesis. In most of this work, de Haas-van Alphen-like quantum oscillations were not observed. In one set of data, however, de Haas-van Alphen-like oscillations having a period of $0.50 \times 10^{-5} \text{ G}^{-1}$ appear to be present.

The published theoretical work was reevaluated. As a result of a large effective Dingle temperature for field emitters, and because the effective masses of carriers in bismuth are anisotropic, the de Haas-van Alphen effect in field emission current could be several times smaller than has been suggested in the literature. The sensitivity of the experiments reported in this thesis was not sufficient to allow unambiguous identification of quantum oscillations at the reduced level. An outline of an experimental procedure suitable for observation of the de Haas-van Alphen-like effect in field emission current at the reduced level is provided in the final chapter.

Search for Quantum Oscillations in
Field Emission Current
from Bismuth

by

Donald Dean Casey

A THESIS

submitted to

Portland State College

in partial fulfillment of

the requirements for the

degree of

Master of Science

June 1968

PORTLAND STATE COLLEGE
LIBRARY

APPROVED:

[REDACTED]

Professor of Physics

[REDACTED]

Head of Department of Physics

[REDACTED]

Dean of Graduate School

Date thesis is presented _____ April 29, 1968 _____

Typed by Helen Marie Casey for _____ Donald Dean Casey _____

Acknowledgements

I would like to thank the members of my thesis committee, Professors Laird Brodie, Gertrude Rempfer, and Donald Wright, for their advice and encouragement during the course of this work. I am especially grateful to Professor Brodie for the many hours he spent introducing me to the excitement of low temperature experimental physics and for his continued willingness to assist in the collection of data. I would also like to thank Mr. James Barter for his assistance with low temperature measurements and Professor M. Takeo for his mathematical check of the results of F. Blatt.

Several members of the technical staff of the Display Devices Department of Tektronix, Inc., contributed to this work. I am grateful for discussions with Dr. Richard E. Coover concerning field emission microscopy during the early stages of this work. I would especially like to acknowledge the very skillful glass artistry of Mr. Keith Deardorf, who prepared the field emission tubes for this research. Finally, I would like to thank Mr. Eugene Hansen for spectrographic and X-ray analysis of some bismuth samples and Mr. Johnnie Schmauder for the donation of a field emission microscope.

TABLE OF CONTENTS

I.	Introduction	1
II.	Materials and Apparatus	5
	Introduction	5
	Materials	9
	Apparatus	21
III.	Experimental Procedure and Results	26
	Procedure	26
	Results	27
IV.	Discussion	54
	Assumptions of the Analysis of Blatt's Theory	55
	Field Emitters and Fermi Surfaces	61
V.	Conclusions and Recommendations	63
	Conclusions	63
	Recommendations	63
	Bibliography	66
	Appendix A: Field Emission Theory	69
	Appendix B: Heating of the Field Emitter	74
	Appendix C: Size Effects	80

TABLE AND FIGURES

TABLE

1(C). dHvA Periods for Electrons and Holes in Bismuth	81
---	----

FIGURES

1. Quantized Field Emission in Bismuth (Theory)	4
2. Growth Tube Construction	12
3. Crystal Growing Apparatus	14
4. Field Emission Tube Design	18
5. Attachment of Emitter	20
6. Cryostat Detail and Sample Placement	22
7. Experimental System	24
8. Fowler-Nordheim Plot for FET-ETM-111	32
9. Rotation Diagram for FET-ETM-111	33
10. Magnetic Field Sweep at 60° for FET-ETM-111	36
11. Magnetic Field Sweep at -10° for FET-ETM-111	38
12. dHvA Period for Oscillations in FET-ETM-111 Current	40
13. Fowler-Nordheim Plot for FET-ETM-112	42
14. Rotation Diagram for FET-ETM-112	43
15. Fowler-Nordheim Plot for FET-ETM-113	45
16. Rotation Diagram for FET-ETM-113	46
17. Magnetic Field Sweep at 0° for FET-ETM-113	48
18. Field Emission from Tungsten and Bismuth Compared	49
19. Fowler-Nordheim Plot for FET-ETM-114	51
20. Magnetic Field Sweep Below λ -Point for FET-ETM-114	52

1(A).	Surface Potential Barrier	73
1(B).	Emitter Model	79

Search for Quantum Oscillations in

Field Emission Current

from Bismuth

Introduction

The concept of a Fermi surface occupies a position of central importance in the theory of metals. It has been known for many years that valuable information about the shape of the Fermi surface (FS) can be obtained from certain electronic measurements made on metals at very low temperatures. Of the measurable direct effects which yield information about the FS, the de Haas-van Alphen (dHvA) and allied effects are probably the most useful.³⁴ In these effects, oscillations, which are periodic in the reciprocal of the magnetic field intensity, of certain properties of metals, such as the magnetic susceptibility or electrical conductivity, provide a direct measure of the extremal cross-sectional area of the FS. Since the pioneering work by de Haas and van Alphen^{9,10} on the magnetic susceptibility of bismuth in the early thirties, the Hall voltage and magnetoresistance in bismuth have also been found to oscillate. After Marcus^{28,29} discovered the dHvA effect in zinc in the late forties, the effort to find the effect in other materials soared. Schoenberg's research survey³³ revealed the dHvA effect in gallium, tin, graphite, cadmium, indium, antimony, aluminum, mercury, and thallium. Subsequently, the dHvA effect was also measured in gold, silver, copper, tellurium, lead, germanium, tungsten

and several other materials. The enthusiasm of the "Fermiologists" and the recent availability of large superconducting electromagnets have continued to spur measurements of the dHvA effect in many materials.

One would expect to observe dHvA-like oscillations in any property of a metal which depends on the density of occupied states at the Fermi level. Thus, it is not surprising that, in addition to the properties which have previously been observed to oscillate in the dHvA manner, it was suggested recently that dHvA-like oscillations should also be observable in field emission current. Blatt⁴ was the first to make this observation. Later, the effect was independently predicted by Gogadze, Itskovich and Kulik.¹⁷

Observation of quantum oscillations (the dHvA effect) in field emission current could be of considerable interest beyond being a mere addition to the ever increasing list of properties of metals which have been found to oscillate. The FS, which is a surface in phase space and not a real space surface, is usually considered to be characteristic of the properties of the electron "gas" in the bulk of the metal. As the size of a metallic sample is made smaller, however, the surface-to-volume ratio increases and, in general, one would expect the surface to affect the properties of the "bulk" material. Indeed, field emission is widely recognized as a powerful tool for the study of real metal surfaces. Usually, however, field emission is used as a tool for the study of the interaction of gases with specific crystallographic faces of metal surfaces, tungsten being the metal most frequently used. It was only recently that field emission was suggested as a means by which

the FS might be studied near real surfaces. If the characteristics of the electron gas are modified near real surfaces, the modifications might very well be studied by means of an observation of quantum oscillations in field emission current.

The research reported herein was undertaken in order to search for quantum oscillations of the dHvA type in field emission current.

Although the dHvA effect has been observed in a wide range of metals, including tungsten which is traditionally used in field emission experiments, bismuth was chosen as the material to be studied in this research because the amplitude of dHvA oscillations in bismuth is relatively large for magnetic fields in the range of ten to twenty kilogauss and because there is an abundance of information concerning the Fermi surface in bismuth from previous bulk measurements. On the basis of the theory presented by Blatt, oscillations with an amplitude of about ten per cent of the total current should be evident at fields of ten kilogauss. The numerical evaluation of Blatt's theoretical result is presented in Fig. 1. The theory is briefly outlined in Appendix A.

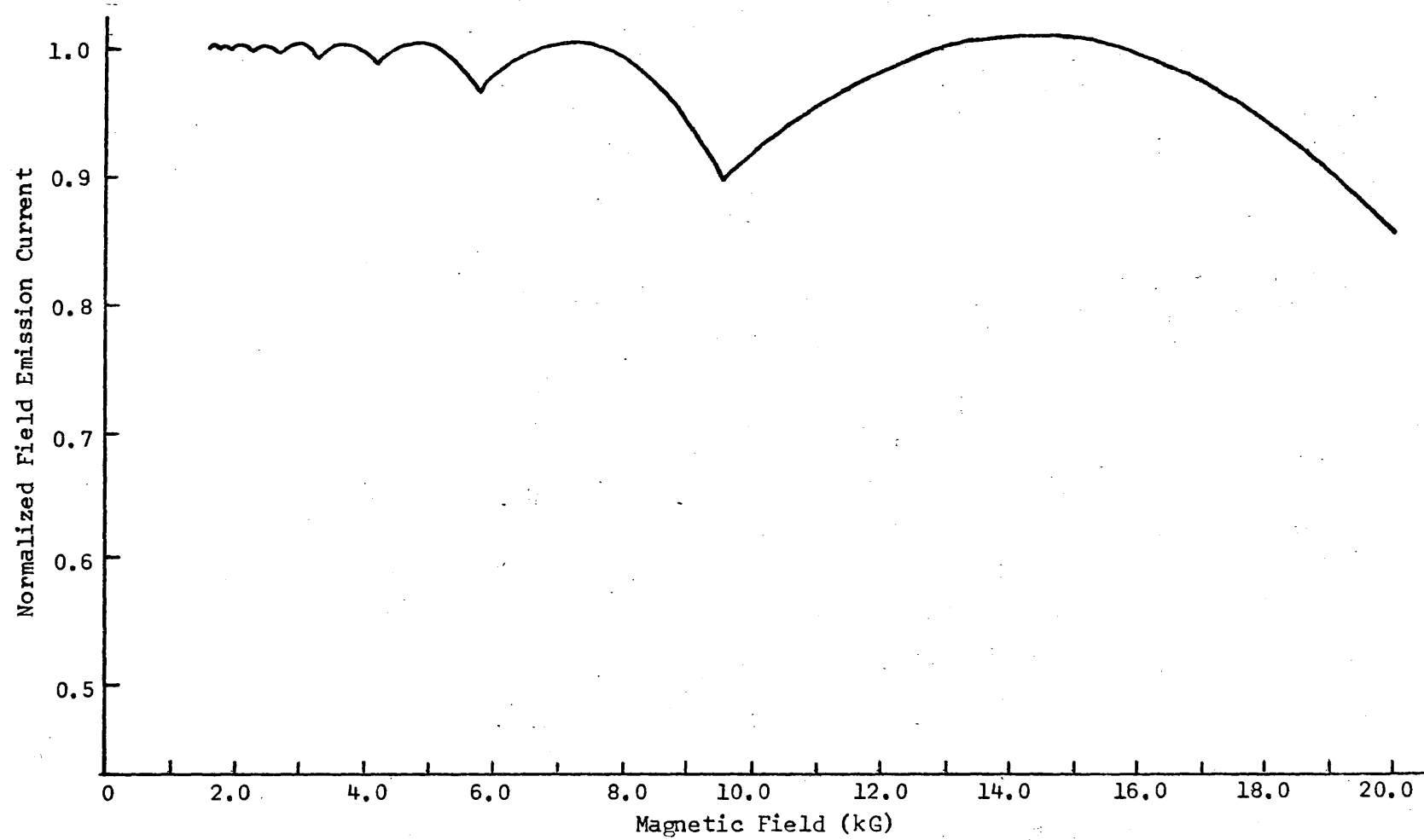


Fig. 1. Quantized Field Emission in Bismuth (Theory)

Materials and Apparatus

Introduction

Most experimental work with field emission is done with tungsten and a few other refractory metals. There is good reason for this. In order to obtain steady field emission currents for field emission microscopy, or for sources of cathode rays, or for surface studies, it is necessary to have not only a good vacuum, but also a well-formed, smooth field emitter of small radius. The means by which clean, smooth emitters are obtained usually involves "flashing" of the tip to a temperature near the melting point of the metal. For tungsten, this is about 3300°C. Flashing of the field emitter causes adsorbed foreign gases to be desorbed and by means of surface diffusion, irregularities on the emitter can be smoothed. The effect of flashing is quite obvious when the image of the field emitter tip is viewed in a field emission microscope during the flashing operation. The main pattern becomes better defined and extraneous patterns due to adsorbed species disappear as the species become desorbed. Another method which can be used to clean field emission tips is that of field desorption.⁸ This involves reversing the field so that the anode is made very negative with respect to the emitter. Adsorbed species are desorbed under the strong field. In order for this method to be used effectively to clean emitters, the emitter must have good tensile strength because of the large stress impressed upon it during field desorption. This technique

is often used in an AC mode, such that viewing and cleaning take place in alternate half cycles. Neither one of the methods normally used to clean field emitters is very applicable when the emitter is made from a material with a low melting temperature, low tensile strength, or both. Bismuth melts at a temperature of 271.3°C. Thermal desorption of surface contaminants is not complete at this temperature. Field desorption was tried on a bismuth field emitter mounted in a field emission microscope during the early part of this work. A clean field emission pattern was never obtained; in fact, it appeared as if the emitter were being pulled apart.

Field emitters are usually made by a controlled etching of the desired emitter material. Both chemical and electrolytic etching processes have been used, with electrolytic etch processes preferred because of the control one is usually able to exercise over the shape and radius of the field emitter. Other techniques, such as grinding, have also been used, but these are generally less satisfactory than non-mechanical processes. Recently, Gomer¹⁸ and Melmed³¹ obtained field emission from a wide range of lower melting materials, including mercury. The clean, smooth emitters were obtained by growing hair-like single crystals of the desired materials in situ in an ultra-high vacuum. Such hair-like crystals are often referred to as "whiskers." Clean patterns were obtained with the technique of field emission microscopy using these emitters. To this author's knowledge, field emission from bismuth has not previously been reported. The fact that bismuth melts at a low temperature suggests that the technique of

whisker growth as a means of obtaining clean field emitters might be quite compatible with this research. There are very few references to the observation of bismuth whiskers in the literature. Recently, however, an article appeared by Mayer³⁰ in which he stated that bismuth whiskers were obtained by growth on thin manganese films. Until recently, most theories of whisker growth have involved a single screw dislocation on the axis of growth. No other growth sites exist on the surface of whiskers. As a consequence, whiskers generally have a much higher tensile strength than their polycrystalline or melt-grown single crystal counterparts. This would be quite desirable for bismuth. On the other hand, it is not known what effect a screw dislocation would have on electron orbits in a magnetic field. Nevertheless, some effort was initially spent in an attempt to prepare bismuth whiskers in vacuum. Mayer's technique was tried at first. Although several attempts were made to grow whiskers on thin evaporated films of manganese, no such whiskers were obtained. An attempt was also made to grow whiskers from the vapor phase on clean, rough surfaces of three mil tungsten wire. Not much effort was made on these two processes because of the difficulty of arranging a vacuum tube suitable both for whisker growth and observation of field emission in a magnetic field. The experimental effort was finally focussed on the preparation of field emitters made from bismuth single crystals grown from the melt. This work will be discussed in detail in the following pages.

The construction of a field emission tube is usually quite simple. In most cases, there are only two electrodes, an anode and the emitter.

Usually, the tubes are built in round bottom pyrex flasks. The bottom of the flask is coated with a transparent conductive coating, over which a phosphor is settled to provide a luminescent indication of emission coming from the emitter. This kind of construction is not necessary, however, and in this research it was not possible. What is essential to acquire good field emission data is a very good vacuum environment. In most cases, where higher melting point metals are used as emitters, the vacuum is obtained by pumping the tubes on well trapped diffusion pumps with simultaneous baking of the tube envelope at temperatures on the order of 450°C. After the pumping is complete, the tube is generally sealed and a getter of some appropriate metal (such as molybdenum, tantalum, or titanium) is flashed in an appendage bulb. Such procedures generally result in ultimate vacuum environments on the order of 10^{-10} Torr. Higher pressures in field emission tubes result in excessive bombardment of the emitter by positive ions, causing instability in the emission current and damage to the emitter.

Several factors dictated the need to deviate from most conventional "state-of-the-art" practices in field emission tube design and processing for this research. Since the field emission tube was to be inserted in a liquid helium cryostat which, in turn, had to fit between the poles of an electromagnet, the envelope of the tube had to be quite narrow. In addition, because of the strength of the magnetic field to be used, no magnetic materials could be used in the construction of the tube. Since bismuth melts at less than 300°C, the usual means for obtaining a good vacuum could not be used. With these

points in mind, a suitable, but non-conventional field emission tube was designed and constructed for this work.

Materials

Preparation of Capillary Bismuth Crystals

Field emitters were formed by chemical etching of capillary bismuth crystals grown in rigid glass molds by the process of normal freezing. The technique is essentially a slight modification of the technique suggested by Bridgeman.⁵ Growth of bismuth crystals in rigid glass molds has previously been found to leave the crystals highly strained due to the fact that bismuth expands upon freezing by about three per cent. Thus, most recent procedures for the growth of large single crystals of bismuth employ a "soft mold" technique. In this work, however, the use of a soft mold was not required because of the very loose requirements on the ultimate size of the single crystal. A monocrystalline structure was only required over a range of about two or three millimeters of the total capillary length and over a diameter of several thousand angstroms. Imperfections in the resultant crystal were usually well identified by the etching process and, in one case, Laue patterns were made of the crystal structure for several millimeters along the length of the capillary. The crystal was found to be well formed as indicated by the symmetry of the Laue patterns and by the crispness of the diffraction image. An attempt was not made to identify the orientation of the crystals in this work, nor were Laue patterns made on all of the specimens used. When the crystal was

obviously strained, as indicated by the appearance of well developed pits or streaks during the process of emitter formation in nitric acid, the etching process was controlled to provide a field emitter with a region avoiding these defects. Thus, it is reasonably certain that the specimens used in this work were in fact monocrystalline over larger portions of the specimen.

The bismuth used in this work was purchased from Cominco Products, Inc., and was of 99.9999% label purity. The bismuth was carefully handled during the critical stages of crystal preparation in order to prevent contamination of the finished specimen. Spectrographic analysis of the bismuth received revealed impurities of copper (3 ppm) and magnesium (1 ppm). Similar analysis made on samples of a crystal grown in a pyrex mold revealed no additional contamination by the mold or etching process.

The mold used for capillary crystal growth was made from pyrex glass. Although the total length of the mold varied from crystal to crystal as the design of the field emission tube changed during the course of this work, the capillary region of the mold retained the same design throughout. The glass tubing (5 mm O.D.) was thoroughly cleaned before any forming was begun. Several lengths of pyrex tubing to be used for molds were completely immersed in a dilute solution of ammonium hydroxide and Alconox (commercial detergent), used as a wetting agent, and set in an ultrasonic unit for a period of fifteen to thirty minutes. After the ultrasonic cleaning, cold deionized water

was allowed to run over the tubes for thirty minutes. The tubes were finally heated in deionized water, rinsed in reagent grade methanol and dried in air on lint-free towels. Care was taken to prevent contamination of the tubes by direct handling during this process. A water-break test performed on each tube indicated that they were free from organic contaminants. That the tubes were free from inorganic contamination was subsequently established by spectrographic analysis of some finished crystals.

A hydrogen-oxygen flame torch with a B #7 tip was used to fabricate molds for crystal growth from the clean tubes. The torch was supported in a ring stand. The tube was rotated rapidly over a hydrogen-rich flame for a distance of several centimeters along the rod, starting at about two centimeters from one end to remove water vapor. The oxygen content of the flame was gradually increased and the heating concentrated near one end of the tube. The tube was allowed to soften until the inner diameter almost collapsed. The tube was then removed from the flame and drawn into a fine capillary of about eight centimeters. The capillary axis was inclined at about five degrees to the tube axis. The end of the capillary was then sealed, leaving a bubble. This is illustrated in Fig. 2(A). Two bends were then made in the capillary as shown in 2(B). Finally, the finished mold was examined under a low power microscope for flaws. The best of several molds prepared was selected from each batch to be used for crystal growth.

Crystals were grown in a vacuum furnace with two separately

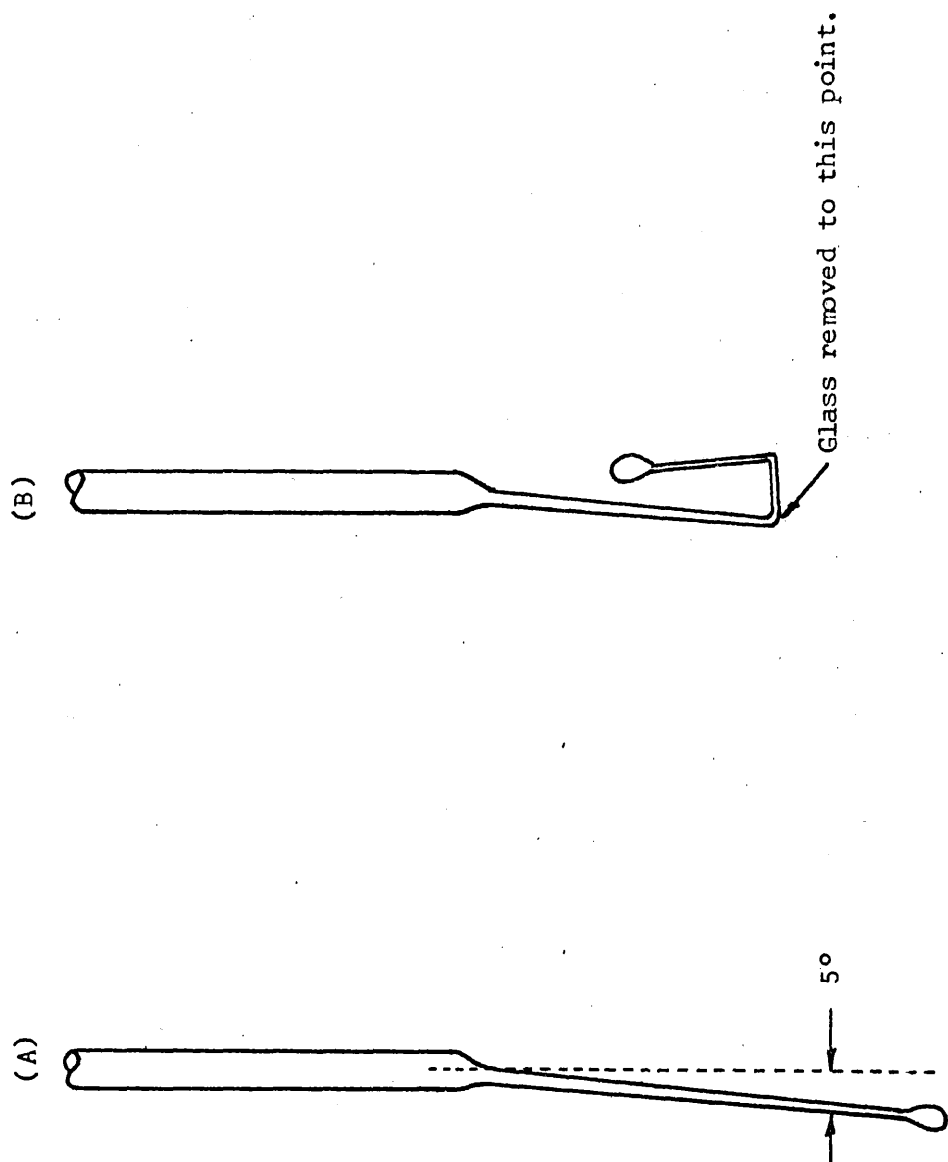


Fig. 2. Growth Tube Construction

controlled hot zones. The design is illustrated schematically in Fig. 3. The temperature profile was determined, for several settings of the separate Variacs used to control the temperature of each furnace, by means of an iron-constantan thermocouple and a Leeds & Northrup Potentiometer.

Crystals were grown by suspending the growth mold in the oven as shown in Fig. 3. Usually, about twenty to twenty-five pellets of pure bismuth were used to grow each crystal; these were placed in each growth tube prior to suspending it in the furnace. The oven was evacuated with a mechanical pump to about five microns for an hour before heating was started. The lower part of the hot zone was brought to temperature equilibrium over a period of several hours; then the upper zone was heated to form the profile I in Fig. 3. The furnace was rapidly backfilled to atmosphere with pure nitrogen gas to force the molten bismuth into the capillary. The lower zone was then slowly cooled (over about eight hours) before the upper zone was cooled. This caused the temperature profile to change along II and III in Fig. 3. The finished crystal was removed from the furnace and stored until used in a field emission tube.

Design and Construction of the Field Emission Tube

The crystals described in the preceding section were installed in field emission tubes after they had been etched to a fine point in a solution of nitric acid. The glass mold was first removed in a bath of

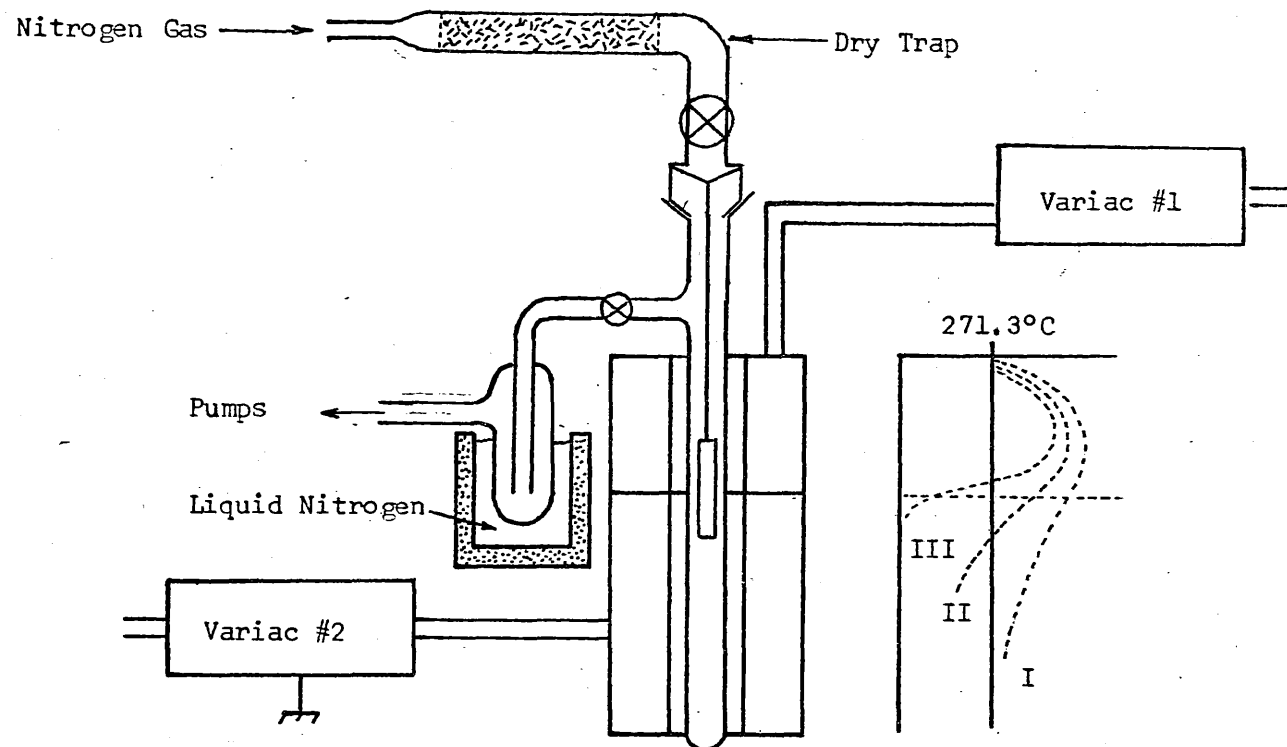


Fig. 3. Crystal Growing Apparatus

concentrated hydrofluoric acid to the point indicated in Fig. 2(B). As the experimental work progressed, some changes were made in the initial design of the field emission tube in order to promote better cooling of the emitters during measurements. The main features of the two primary tube designs are illustrated in Fig. 4. Deviations from either one of these designs in a particular tube will be mentioned along with the results of measurements made on the tube in Chapter III.

The tube envelope (a) was made of pyrex glass, having a diameter of thirteen millimeters. Although an aluminosilicate glass is less permeable by helium, pyrex has been found to be satisfactory. We experienced no difficulty with leakage of helium through the walls during the short times in which the tube was immersed in the liquid. Care was taken to remove helium from the surrounding atmosphere before the tube warmed to room temperature after an experiment. A Dewar seal (b) at the top of the tube allowed a passage for liquid helium into the tube interior and thus into contact with the cathode lead (c) coming from the crystal. It is not known whether the helium actually entered the reentrant portion of the tubes for most of the experiments. In the last two experiments, however, the helium temperature was reduced below the lambda point. The "creep" effect probably allowed the helium to migrate into the interior of the tube for these measurements. The tube shown in Fig. 4(B) was used for the measurements below the lambda point. In the tube of design (A), a bead of uranium glass (d) was used to maintain vacuum integrity. The glass was formed on the tungsten cathode lead and then sealed to the tube envelope after

attachment was made to the bismuth crystal with the cathode lead. The first tube of design (A) did not include this bead and it was found that helium leaked into the tube, probably through the bismuth-to-glass seal at low temperature. The anode (e) was fabricated from titanium or molybdenum and was spot-welded to a tungsten support. The support was also beaded with uranium glass and sealed directly to the pyrex envelope. In design (B), the large anode was sometimes replaced by a tungsten field emitter, with the axes of the tungsten emitter and the bismuth emitter nearly coincident. In these tubes, the voltage could be reversed to compare field emission from tungsten with that from bismuth. Tubes of both designs also included a guard ring (f) after the first tube. In most tubes of either design, the guard ring consisted of a piece of aluminum foil taped to the outer wall of the envelope. This arrangement was found to be quite satisfactory. Two of the type (B) tubes had guard rings of Kovar sealed in the outer wall. This process, however, was tricky, requiring a graded seal of pyrex to uranium glass to Kovar sealing glass and finally to the Kovar. The carbon content of the Kovar affects its expansion coefficient considerably and thus the preparation of the Kovar is critical for metal to glass seals to be used over a wide temperature range. In addition, Kovar goes through an irreversible phase change below -80°C which causes the thermal expansion coefficient to vary considerably on cooling and heating cycles. Thus, difficulty with seal integrity was encountered when these tubes were brought to room temperature after a measurement at 4.2°K . In tubes of design (B), a few features differed

from type (A) tubes. Thus, the reentrant portion of the tube and the crystal mold were not one continuous piece. The reentrant portion ended in a dome of uranium glass (g) with a 0.060" diameter tungsten pin sealed to this end (h). This arrangement allowed liquid helium to come directly into contact with not only the cathode lead (c), but also with the tungsten pin which was soldered directly to the bismuth crystal (i). The tubes were all evacuated through the end nearest the emitter.

The tubes were usually built in two sections. The last tube, which incorporated a coating of tin oxide, was built in three different pieces. The outer envelope of the tube was nearly the same for each tube (with the exception of those two tubes which incorporated a Kovar guard ring). Thus, several were made at a time. The lengths of the tubes varied, those of design (B) being several inches longer than those of design (A). The cleaning process was not so rigorous with the envelope as it was for the capillary tubing. The main envelope was domed at one end and flattened with a carbon tool. Two holes were blown in this end, to which were then attached the pumping tubulation shown in Fig. 4 and a smaller diameter tube to accept the anode support.

The anode was made from titanium, or molybdenum sheet stock of 0.006" to 0.008" thickness. A strip of the sheet, usually about one centimeter high, was bent over a rod and then cut to form a half cylinder. This piece was spot-welded to a piece of tungsten wire which had been beaded with uranium glass and cleaned in a dilute solution of sodium hypochlorite to remove oxides. The anode was electropolished

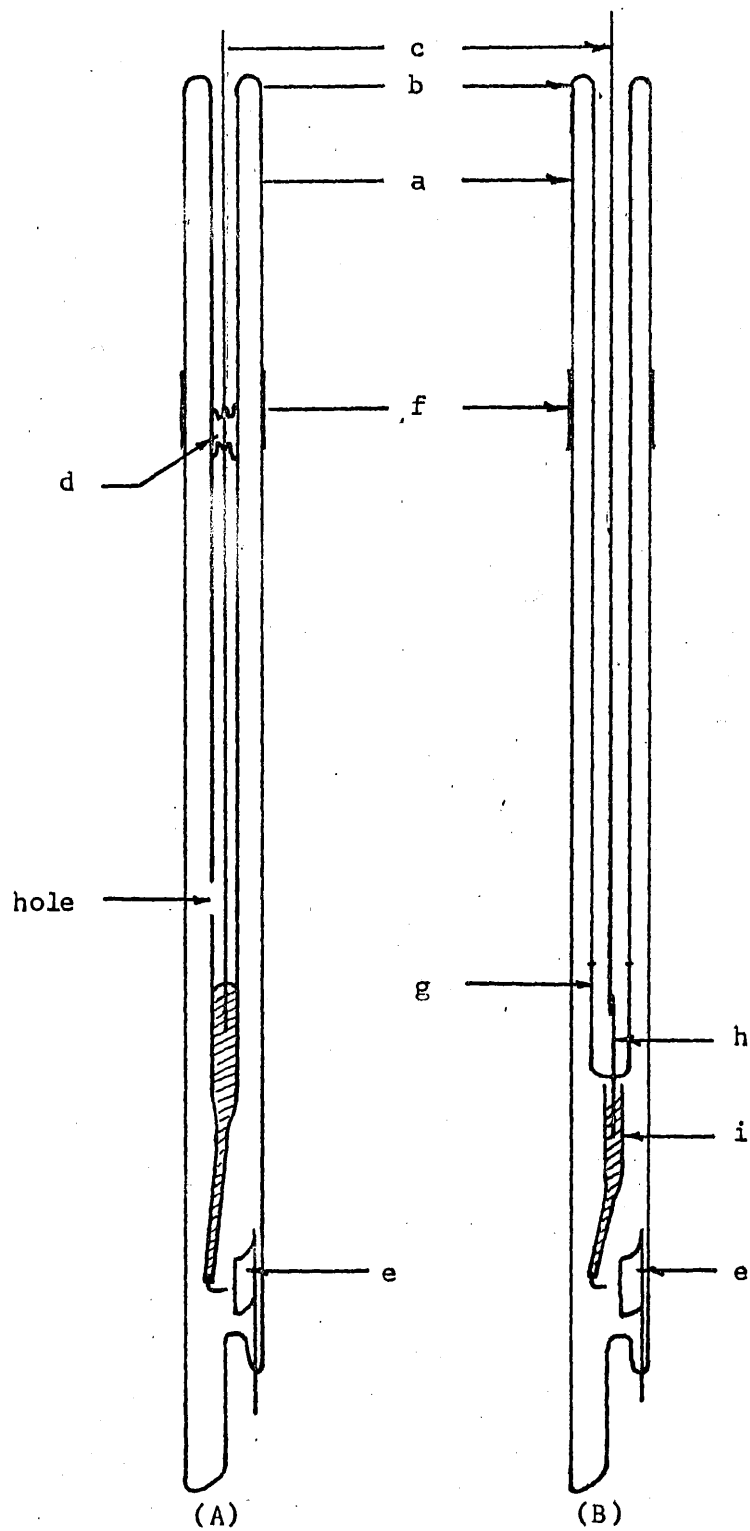


Fig. 4. Field Emission Tube Design

in a solution of 60% phosphoric acid, 20% hydrofluoric acid and 20% methanol at several amperes until a smooth, shiny finish was developed on the anode. Finally, the anode was cleaned in NaOCl, rinsed in deionized water and methanol and dried in air on a lint-free towel. The finished anode was then sealed to the envelope.

In tubes of type (A), a Dewar seal was made directly to the top of the crystal mold. The outer portion of the Dewar seal (13 mm O.D.) was cut off at a length of two inches from the top of the tube. In tubes of type (B), the Dewar seal was made to a section of eight millimeter tubing (larger than the inner tubing used for the tubes of design (A)) which had been domed with a three centimeter length of uranium glass. The domed end was then removed just above the pyrex-uranium seal, and a 0.060" tungsten pin inserted in the domed end (Fig. 5). A piece of 304 stainless steel (the cathode lead in (B) tubes) was spot-welded to the tungsten pin prior to resealing of the domed end to the rest of the reentrant portion of the tube.

In tubes of type (B), the crystal was attached to the tungsten pin (which had been cleaned of oxides in NaOCl and electropolished to develop a smooth, shiny surface) by locally melting the bismuth in the mold and adjusting the crystal by hand onto the pin. The arrangement is illustrated in Fig. 5. The glass was etched away from the bismuth at the tip with concentrated hydrofluoric acid. The tip was then etched in a solution of nitric acid (about 80%). As the etching progressed, the shape of the emitter was monitored by viewing under a microscope. When an emitter of the desired geometry was developed, the

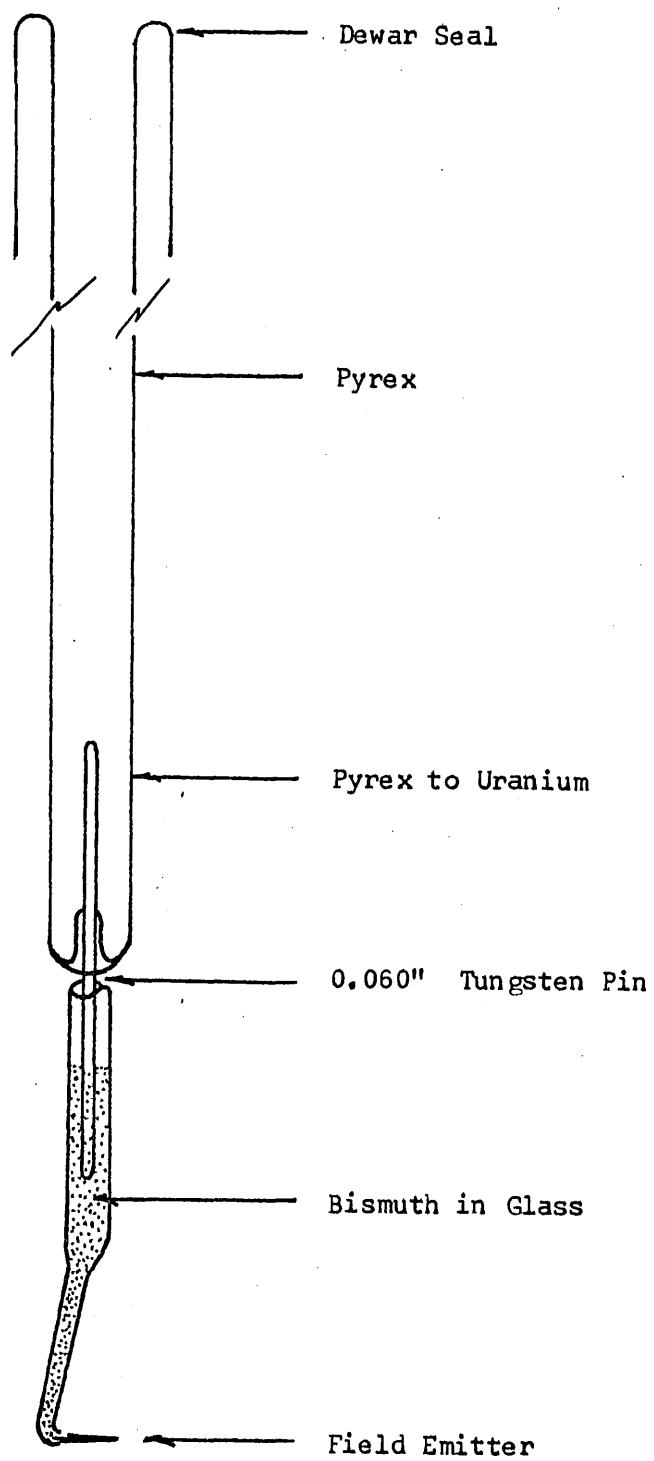


Fig. 5. Attachment of Emitter

emitter was installed in the outer envelope by bringing the two pieces of the tube together on a lathe. The final glass seal was made by hand torch on the lathe.

The tubes were evacuated to a pressure of 10^{-6} Torr on a charcoal trapped oil diffusion-pumped system. The tubes were held at 150° to 175°C during several hours of pumping. The tubes were sealed at a position about two inches below the emitter and removed from the pumps.

Apparatus

The liquid helium cryostat with the field emission tube in place is illustrated in Fig. 6. The perimeter of the cryostat is filled with liquid nitrogen to provide a shield for the liquid helium which is transferred through an insulated tube to the inner portion of the cryostat. The cryostat used in this work was not constructed with a liquid nitrogen shield surrounding all portions of the inner Dewar containing helium. This design permitted more work space in the "finger", but caused the hold-time of the cryostat to be rather short. The helium level usually fell below the guard ring on the field emission tube after about one hour. Experimental work was discontinued when this occurred (although liquid helium has a high dielectric strength, electrical breakdown occurs easily in the gaseous helium region above the liquid; thus, experimentation could not be continued once the guard ring was exposed through the gaseous helium to the high voltage).

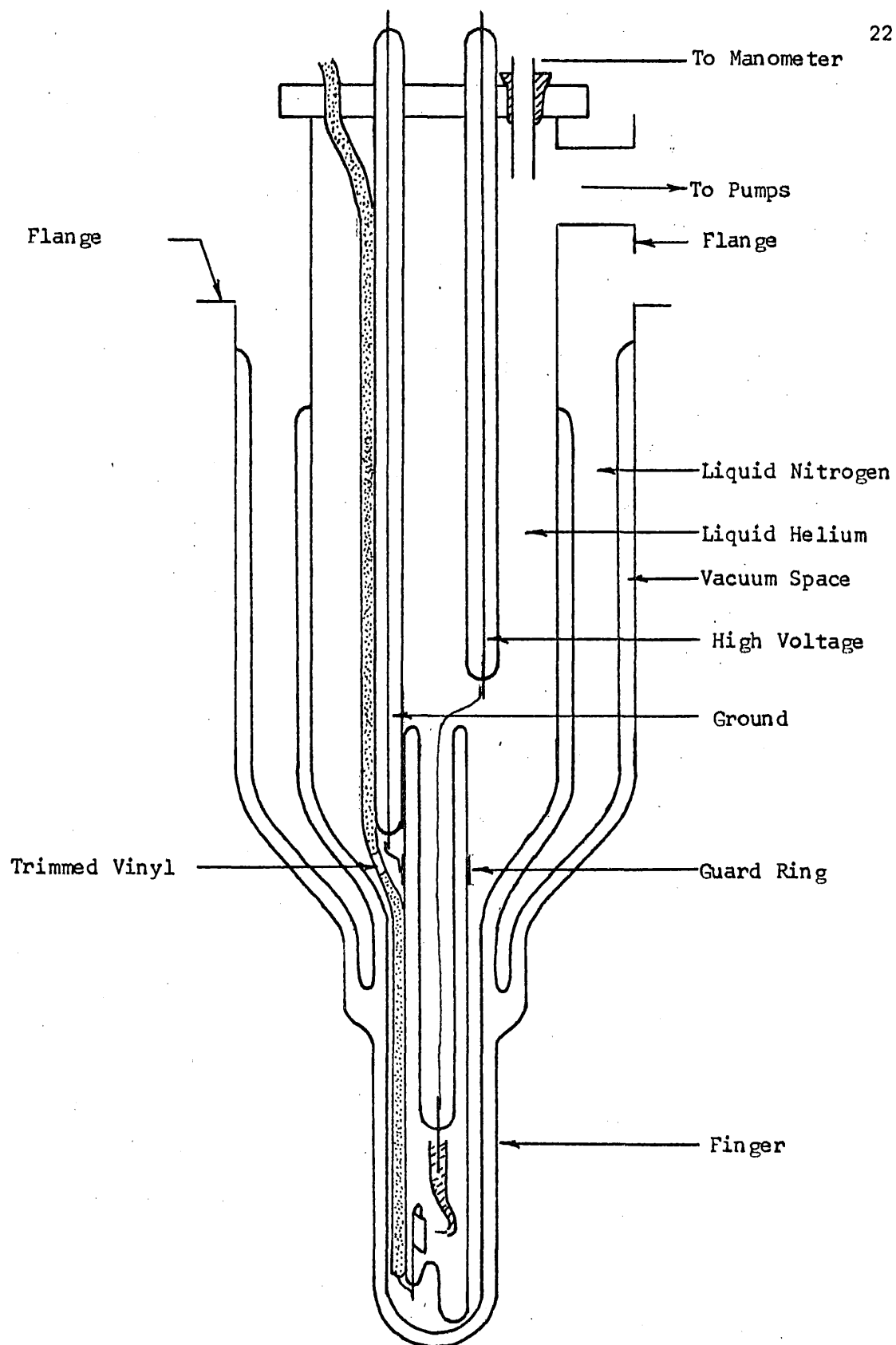


Fig. 6. Cryostat Detail and Sample Placement

In order to prevent a gas discharge from occurring in the region above the liquid helium level, high voltage was introduced into the Dewar through evacuated leads. These were constructed of uranium glass tubing with a tungsten lead running along the axis. The high voltage leads entered through vacuum tight seals at the top of the cryostat. The details of the top are not shown in the illustration. The field emission tube was mounted to one of the high voltage leads as shown in Fig. 6 by means of masking tape. Connection was made to the cathode lead and the guard ring by means of spot-welds. Connection to the anode was made through a continuous run of coaxial cable so that shielding was accomplished to within about two inches of the anode. When coax was not used, electrical noise became a problem. Leakage currents along the glass were reduced to a very low level by means of the guard ring. Also, the vinyl sheath of the coaxial cable was trimmed away (Fig. 6) to prevent leakage currents from reaching the anode lead by means of the coax. When these precautions were taken, electrical noise was reduced to a level substantially below the size of the signal we wished to detect.

The cryostat could be pumped and the pressure measured for experimental work below 4.2°K . Mechanical pumps were used to pump below the lambda point. The pressure was monitored with mercury and oil manometers. The lambda transition could also be detected by viewing the helium meniscus through an unsilvered strip on the cryostat wall.

The entire experimental system is illustrated in Fig. 7. Field

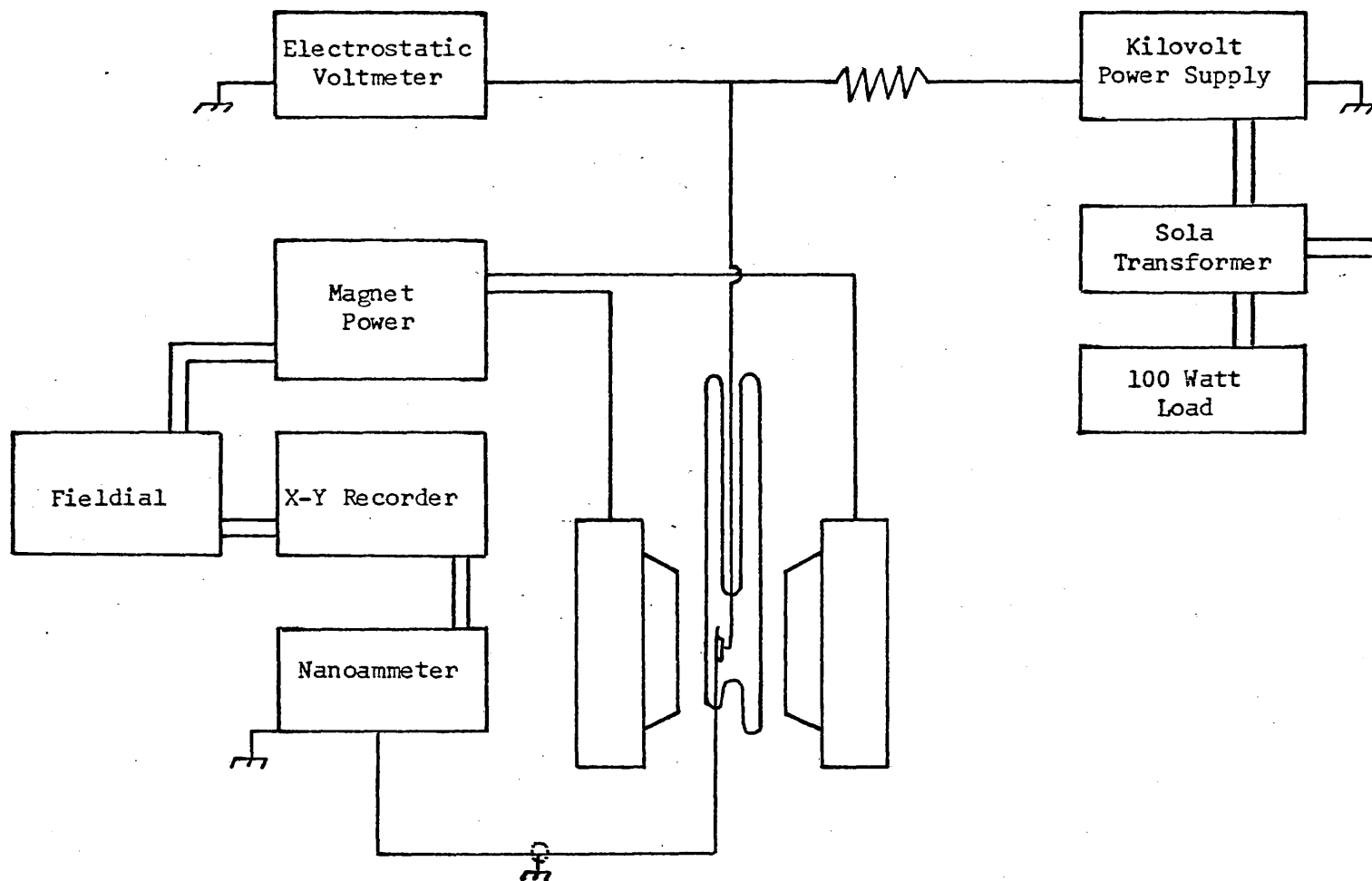


Fig. 7. Experimental System

emission current was usually monitored in the anode lead with a Hewlett-Packard Microvolt-Ammeter. The current was automatically recorded on a Mosley Model 7000A X-Y recorder as a function of magnetic field intensity. Voltage was obtained from a Sorensen high voltage supply. Line voltage was regulated in the last experiments with a Sola constant voltage transformer. The high voltage was measured with an electrostatic voltmeter (Sensitive Research Model ESH). A Varian 12 inch electromagnet, Model V 3603, and Fieldial power supply was used to obtain magnetic fields to 20.4 kG. The field could be swept at several rates; most measurements were made with a 2.5 minute sweep from 70 G (residual field) to 20 kG. On a few occasions, smaller portions of the current versus magnetic field strength spectrum were monitored by expanding the field to 2.5 kG for the 2.5 minute sweep.

Experimental Procedure and Results

Procedure

With the sample in place in the cryostat as shown in Fig. 6, liquid helium was transferred to the inner Dewar after the nitrogen shield was filled and the "finger" had been pre-cooled with liquid nitrogen. Due to the short hold-time of the cryostat used in this work, measurements were begun immediately upon completion of the helium transfer. High voltage was slowly applied to the field emitter until current was detected. Since emission was usually erratic at the beginning of an experiment, the voltage was usually raised slowly until several microamperes of cathode current were drawn. An I-V relationship was then recorded as the voltage was lowered to a point at which only a few tenths of a nanoampere were being drawn. Usually, two or three determinations were made of the current-voltage relationship before other measurements were made.

With the field emission current set to a predetermined value, the magnet was rotated with respect to the emitter axis. A field of ten kilogauss was used for this measurement. The effect of the field rotation was found to be non-symmetrical with respect to the axis of the emitter and considerably influenced by the geometry of the anode. Although this latter effect suggests electron optical causes rather than an anisotropy in the solid state properties of field emission from bismuth, some speculative discussion concerning anisotropy is

included in the remarks to follow.

Finally, current dependence on magnetic field strength was measured for a range of initial currents and magnetic field orientations. At the completion of an experiment, a final I-V relationship was made and compared with the initial relationship in a Fowler-Nordheim plot of the data.

Results

Field Electron Emission Microscopy of Bismuth

A bismuth field emitter was mounted in a conventional field emission microscope (FEM) and processed on an oil diffusion-pumped system. The FEM was sealed off from the vacuum system when the pressure reached 5×10^{-6} Torr. Operation of an appendage ionization gauge reduced the pressure to 5×10^{-8} Torr. Finally, a portion of the tube was immersed in liquid nitrogen and operated. An image started to develop on the viewing screen when about 1.5 kV was applied. A typical pattern did not show any particular symmetry. Several attempts were made to obtain a clean emission pattern by resistive heating of the emitter and by field desorption techniques, all without success. Perhaps only in situ growth of bismuth field emitters, such as Melmed and Gomer^{18,31} have used for other materials, will provide field emitters sufficiently free from contamination to result in field emission patterns representative of a clean bismuth substrate.

Although clean field emission patterns will probably not be readily obtainable with field emitters etched from bismuth crystals grown from the melt, this should not (with our present understanding) influence the observation of the de Haas-van Alphen effect in such samples. The dHvA effect would, of course, be influenced by the degree of bulk crystalline perfection at the tip.

Experimental Tube FET-ETM-107

This was the only tube constructed in such a manner that direct contact was made to liquid helium by the crystal when readied for testing. After initial testing, it was apparent that helium gas had leaked into the tube, probably through the glass-to-metal seal. Thus, further construction of this type was not attempted. No significant data were collected from this crystal due to the poor vacuum conditions.

Experimental Tube FET-ETM-111

A field emission tube of the type shown in Fig. 4(A) was used to test this crystal. In order to relieve stress from the bead (Fig. 4(A)) region, which was thought to contribute to the failure of the previous tube, a five mil tungsten wire was used for the cathode lead. Previously, a fifteen mil lead had been used for the cathode lead. This lead was also gold plated to reduce the possibility of its oxidation during the process of connecting it to the bismuth. Other

processing was as has been described previously.

A portion of the crystal (not the same portion as was subsequently used for field emission) was examined by back-reflection X-ray diffraction, by Gene Hansen of the Tektronix Analytical Chemistry Laboratory. The Laue pattern obtained indicated a well crystallized sample over a region of several millimeters. Crystal orientation was not determined. During the emitter formation process, some strain lines appeared in the crystal, separated by about two millimeters. The tip was formed between two of these strains; thus, it is felt that the crystal was probably well formed for a distance of about two millimeters in this sample.

It became apparent toward the end of this work that a knowledge of the geometry of the anode was very important in order to explain some of the operating characteristics of the tubes tested. During the course of the work, no attempt was made to hold the dimensions of the anode constant. As a matter of fact, this was fortuitous in that we might have mistaken an electron optical characteristic for a solid state effect had the anode geometries all been identical. As it is, however, it is felt that some of the observed operating characteristics were purely electron optical, although exact numerical data could not be obtained due to some uncertainty with respect to the exact geometry of anodes in each tube. In this device, the anode was fabricated from molybdenum and was formed by bending a strip of six mil molybdenum, ten millimeters wide, over a rod of about five millimeter diameter. The strip was then trimmed to form a half-cylinder. When assembled in

the tube, the end of the field emitter tip fell within the edge boundaries of the anode. As with other anodes, the anode was electro-polished and cleaned before assembly into the field emission tube.

Measurements were first made on this tube with the inner Dewar filled with liquid nitrogen rather than liquid helium; thus the ultimate pressure in the tube was probably not less than 10^{-8} Torr. This is higher than one normally operates a field emission tube because of the excess noise from bombardment of the emitter by residual gases. Emission initially started at approximately 1.2 kV, but crept up to 3 kV after several runs, suggesting that the emitter was being dulled by operation. The emission was noisy, so that good current-voltage data were initially difficult to obtain. The noise was probably due, in part, to the dirty condition of the emitter. In addition, it was found that external noise, such as changes in capacitance to the measuring leads, by movement of personnel, also contributed to the over-all difficulty in obtaining good Fowler-Nordheim plots. The Fowler-Nordheim equation is of the general form (Appendix A)

$$J = A'E^2 \exp (-B'/E) \quad [1]$$

Throughout this thesis, the author has assumed the necessary and sufficient condition for field emission to be that a plot of $\log I$ vs $1/V$ be linear over several orders of magnitude for relatively small changes in V , where I is the total emitted current and V is the applied voltage.

Several experiments were made with this tube and crystal once

external noise had been eliminated by proper shielding. In all subsequent work, the tube was always immersed in liquid helium. A typical Fowler-Nordheim plot of the I-V data from this crystal appears in Fig. 8. It is seen to be linear over several orders of magnitude. Although the slopes changed only slightly from measurement to measurement, the curve did not always occupy the same voltage range. This would be expected if the crystal tip were being modified during operation by vacuum arcing or other mechanisms. In all of the work reported here, where the slopes of the curve taken before and after the measurement of magnetic field effects, both the slope and position of the I-V curve were essentially unchanged during a given experiment.

With the magnetic field set at ten kilogauss and a small field emission current being drawn from the bismuth emitter, the magnet was rotated through plus and minus ninety degrees in a plane including the length of the crystal. The result of this rotation is shown in Fig. 9. It is interesting to note that if the points ranging from 0° to $+70^\circ$ were to be translated to the range -90° to -20° , the two sets of points would define the same curve. The physical orientation of the emitter was parallel to the magnetic field to within $\pm 5^\circ$ at $\theta = -10^\circ$ in this experiment. A complete explanation of this symmetry in the rotation is difficult since the crystallographic orientation of the emitter is not known. If emission were coming from the apex of the emitter, as is expected, then one would expect the rotation diagram to have mirror symmetry as the magnetic field is rotated about the emitter. This kind of symmetry is not in evidence here. On the other hand, if

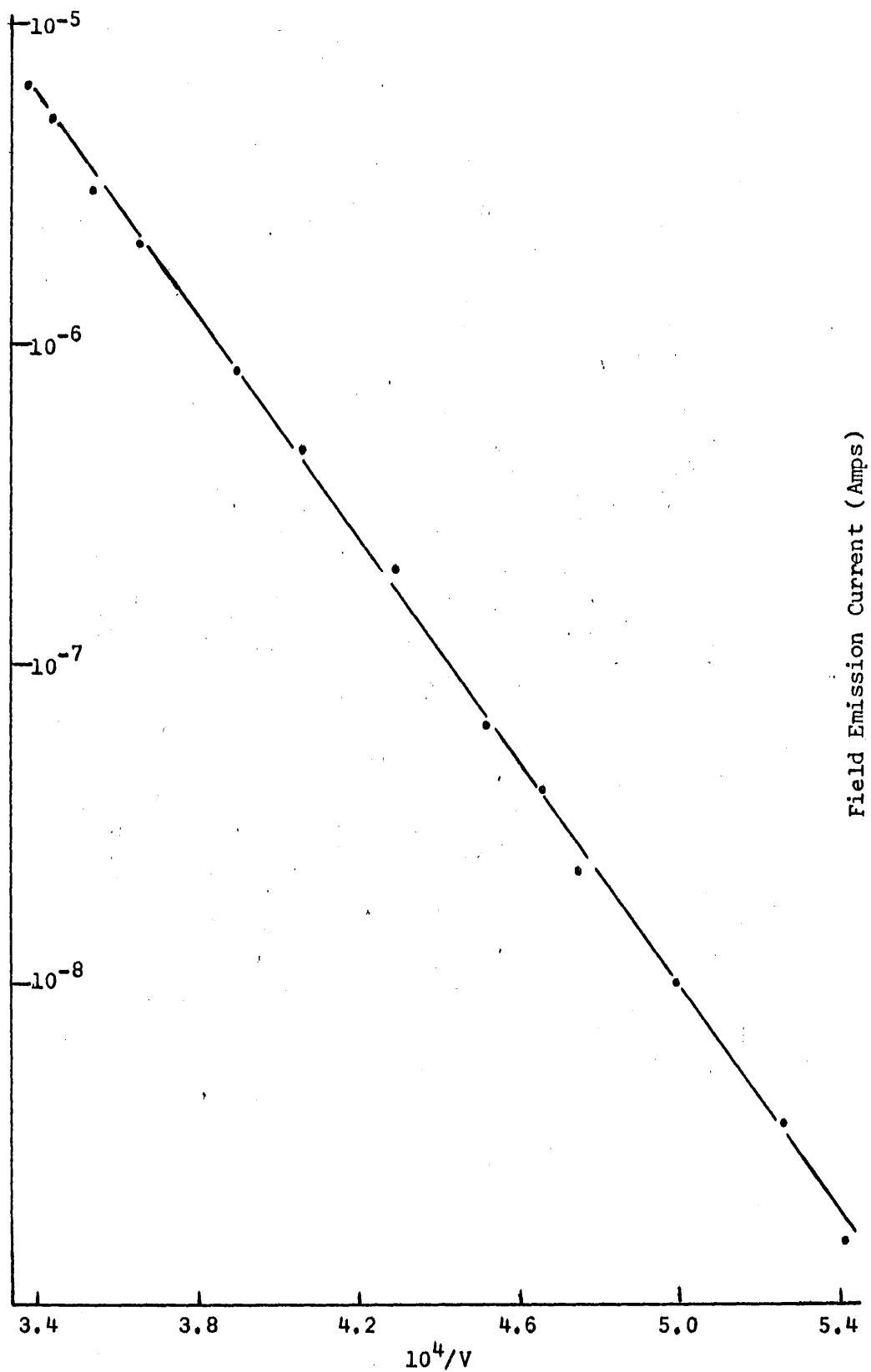


Fig. 8. Fowler-Nordheim Plot for FET-ETM-111

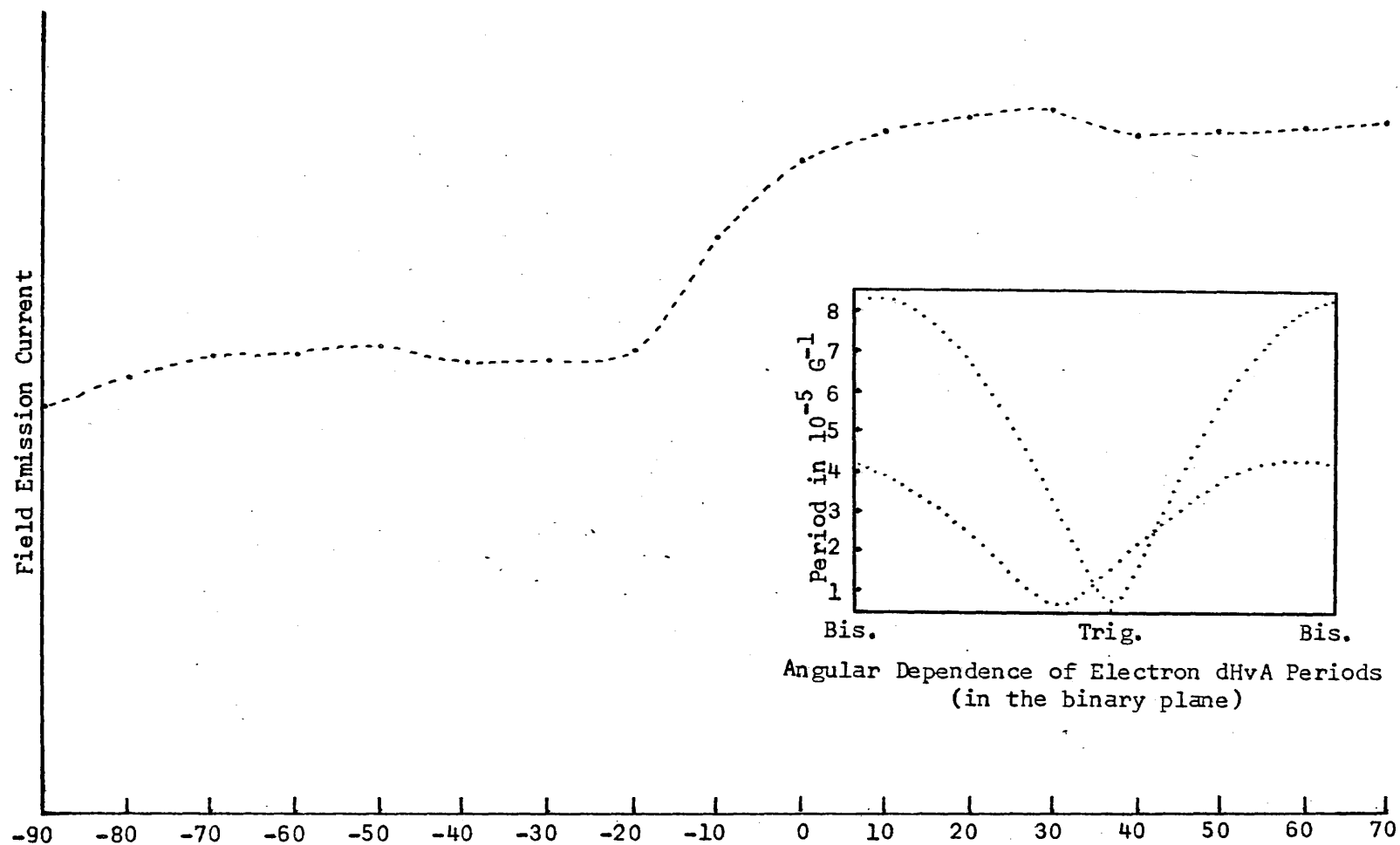


Fig. 9. Rotation Diagram for FET-ETM-111

the variations in the rotation were due to solid state anisotropy, or, if emission were coming from an off-axis crystallite, then the rotation diagram would not necessarily be expected to have mirror symmetry. In the case of a solid state effect, the lack of mirror symmetry would be especially true if the axis of the emitter did not coincide with one of the major axes of the crystal, i.e., binary, bisectrix, or trigonal.

Consider the insert in Fig. 9, data obtained by Bhargava.² The periods of dHvA oscillations have been obtained for electrons in the binary plane as the magnetic field is rotated 180° from a bisectrix axis through the trigonal axis. The periods are seen to change considerably and since the dHvA period is a measure of extremal cross sectional area of the Fermi surface perpendicular to the B direction, the real-space orbit size must also change in the sample as θ is changed. If the field emitter axis were to correspond to a crystallographic axis intermediary between the bisectrix and the trigonal axis, then the kind of symmetry seen in our rotation diagram might be expected; that is, as the magnetic field is rotated to $+\theta$, the orbits might become smaller, causing an initial increase in the field emission current, while rotation to $-\theta$ would increase the size of the orbits and tend to reduce emission initially. Finally, it is also interesting to speculate about the symmetry which might be seen in the rotation diagram if the change in emission with rotation represented an observation of the symmetry of the hole ellipsoid in bismuth. Since the hole ellipsoid is symmetric about the trigonal axis of bismuth, if

the emitter were to grow with its axis perpendicular to the trigonal axis, then rotation of the field in the plane of the emitter would not change the size of carrier orbits. If the emitter were to have grown in the direction of a crystal axis in the trigonal-binary, or trigonal-bisectrix plane, however, rotation of the magnetic field in the axis of the field emitter would change the carrier radius, and the symmetry of the rotation diagram would depend on the growth direction.

Although only a speculative analysis of the rotation diagram can be made, having noticed the unusual symmetry, this was taken into account during the remainder of the experiment and therefore current versus magnetic field intensity data were acquired for a large number of field orientations. The effect of increasing the field from 70 G to 20 kG with $\theta = 60^\circ$ is illustrated in Fig. 10. In the upper curve, the field emission current was monitored in the cathode lead, while in the lower curve the current was measured at the anode with the field emitter at a negative voltage with respect to ground. The two curves are essentially the same, although the upper curve is less noisy. The fine structure is not reproducible and much of this noise was eliminated in later experiments by the use of a Sola regulator in the high voltage A.C. line.

It was initially felt that we might distinguish between solid state and electron optical causes for the initial drop in current by monitoring current in the anode and cathode leads separately. It was felt that if an electron optical cut-off were the cause of the initial decrease, then, since the total emitter current could be monitored in

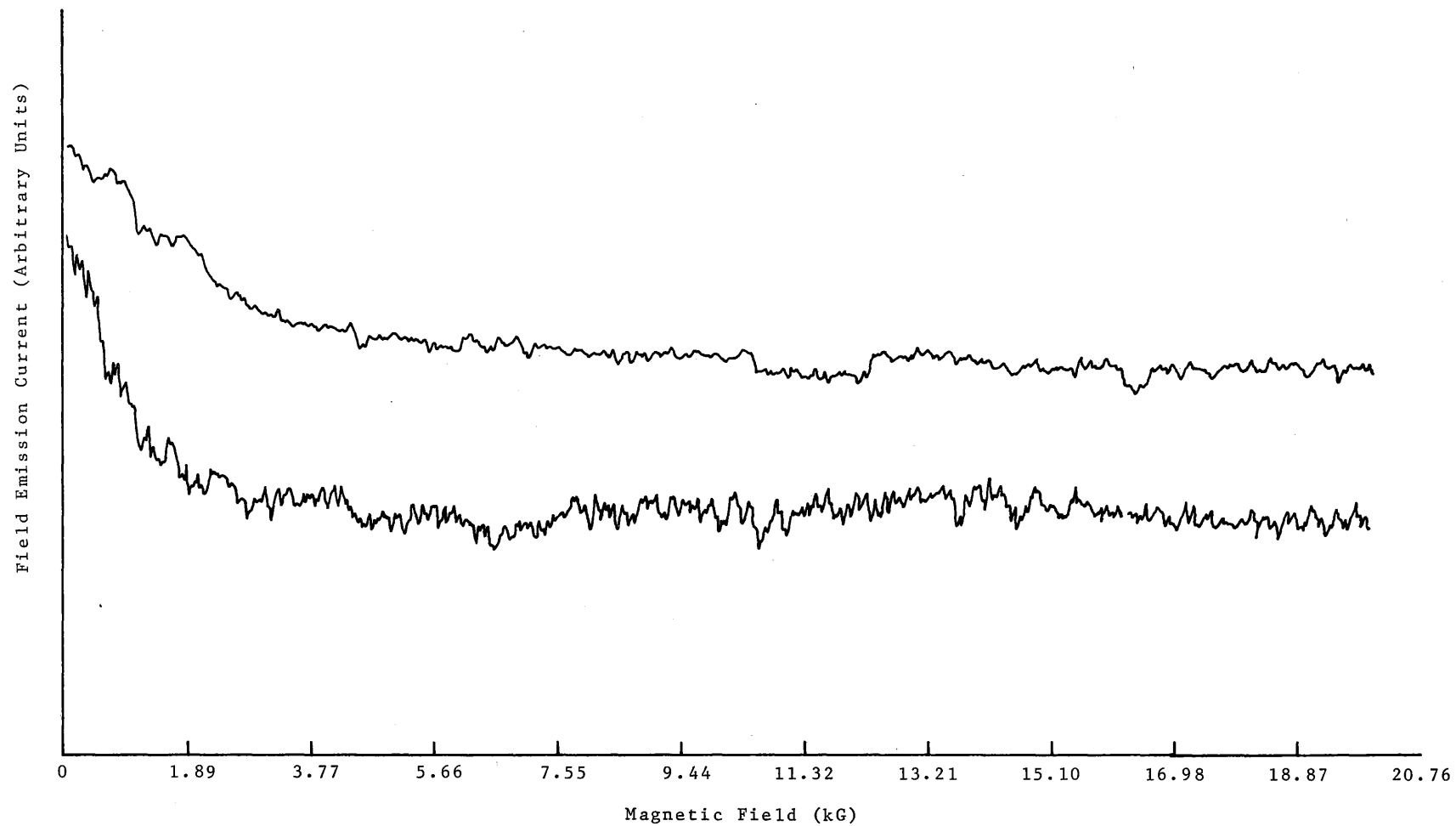


Fig. 10. Magnetic Field Sweep at 60° for FET-ETM-111

the emitter lead with essentially no current returning to the emitter because of the low probability for penetration back through the surface potential barrier, the lack of an observation of an initial current decrease would confirm the effect as electron optical in nature. The continued presence of the initial decrease in emission with increasing B would have caused us to believe that the effect was solid state in nature. As can be seen from Fig. 10, the initial decrease in current did persist but the drop in current proceeded more slowly. The drop can probably best be explained by charging of the field emission tube walls by electrons diverted from the anode by the magnetic field and consequent reduction of the electric field at the emitter. This hypothesis seems to be confirmed by the fact that the initial current drop phenomenon disappeared when the inner wall of the field emission tube was coated with a conducting film which was electrically connected to the anode.

Although the noise level was reasonably high in both curves of Fig. 10, the dHvA effect at the 10% level would have been detectable. Ten per cent limits are drawn for each curve at the high field end. The curve in Fig. 11 was obtained for a B-field orientation of $\theta = -10^\circ$, essentially parallel to the axis of the field emitter. The general appearance of the curve is the same as that of the curves at $\theta = 60^\circ$. Consider, however, the high field end of the curve. Starting at about 15 kG, some small oscillations develop which were not present in the previous data. By placing tracing paper over the original data and drawing an "average" line through the noise, the smooth curve just

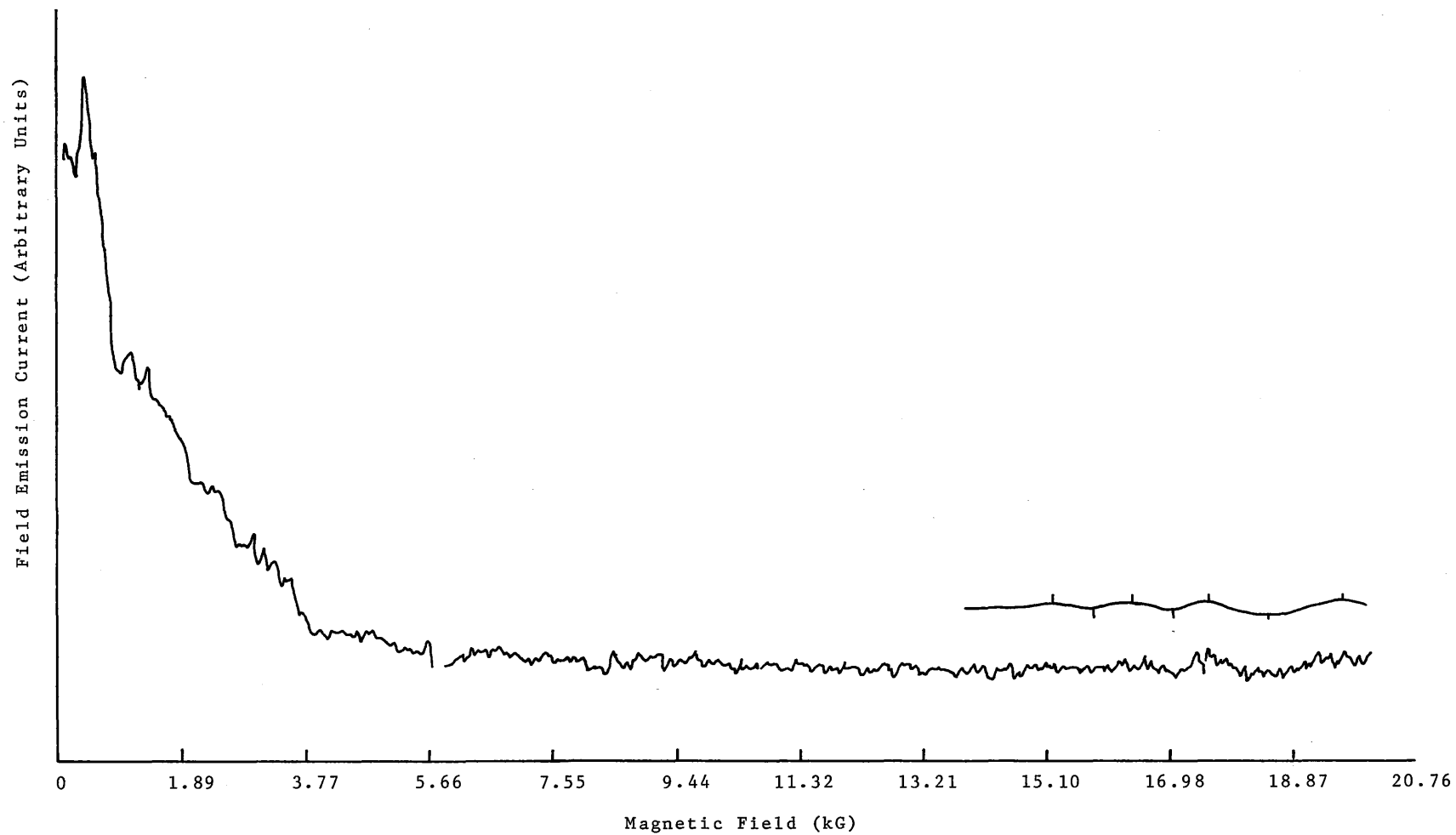


Fig. 11. Magnetic Field Sweep at -10° for FET-ETM-111

above the original data was obtained. These data look very much like the dHvA effect. If it is, the oscillation should be periodic in B^{-1} . Numbering the high and low points of the oscillatory portion of the curve, calling the peak at the highest field number one, these numbers were plotted against B^{-1} in Fig. 12. It is quite evident that the oscillation is periodic in B^{-1} , having a period calculated to be $0.50 \times 10^{-5} \text{ G}^{-1}$. Thus, these oscillations look very much like the dHvA effect in field emission current. This is the effect for which we were searching. It is interesting to compare the value obtained here for the period of the oscillations with literature values. Bhargava² found a period of $0.45 \pm 0.02 \times 10^{-5} \text{ G}^{-1}$ for the hole ellipsoid in bismuth when the B-field was oriented along an axis perpendicular to the trigonal axis. The single hole ellipsoid in bismuth is symmetric with respect to rotation about the trigonal axis. Thus, our value for $P(1/H)$ compares very favorably with that obtained by Bhargava. It is unfortunate, however, that this oscillation was not noticed at the time the experiment was being conducted and so the data were not reproduced at the time.

Experimental Tube FET-ETM-112

This crystal was mounted in a tube of the type shown in Fig. 4(B). The aluminum foil guard ring was replaced by a Kovar cylinder sealed in the glass envelope. This provided a complete guard between high voltage and low voltage ends of the tube. During the course of the

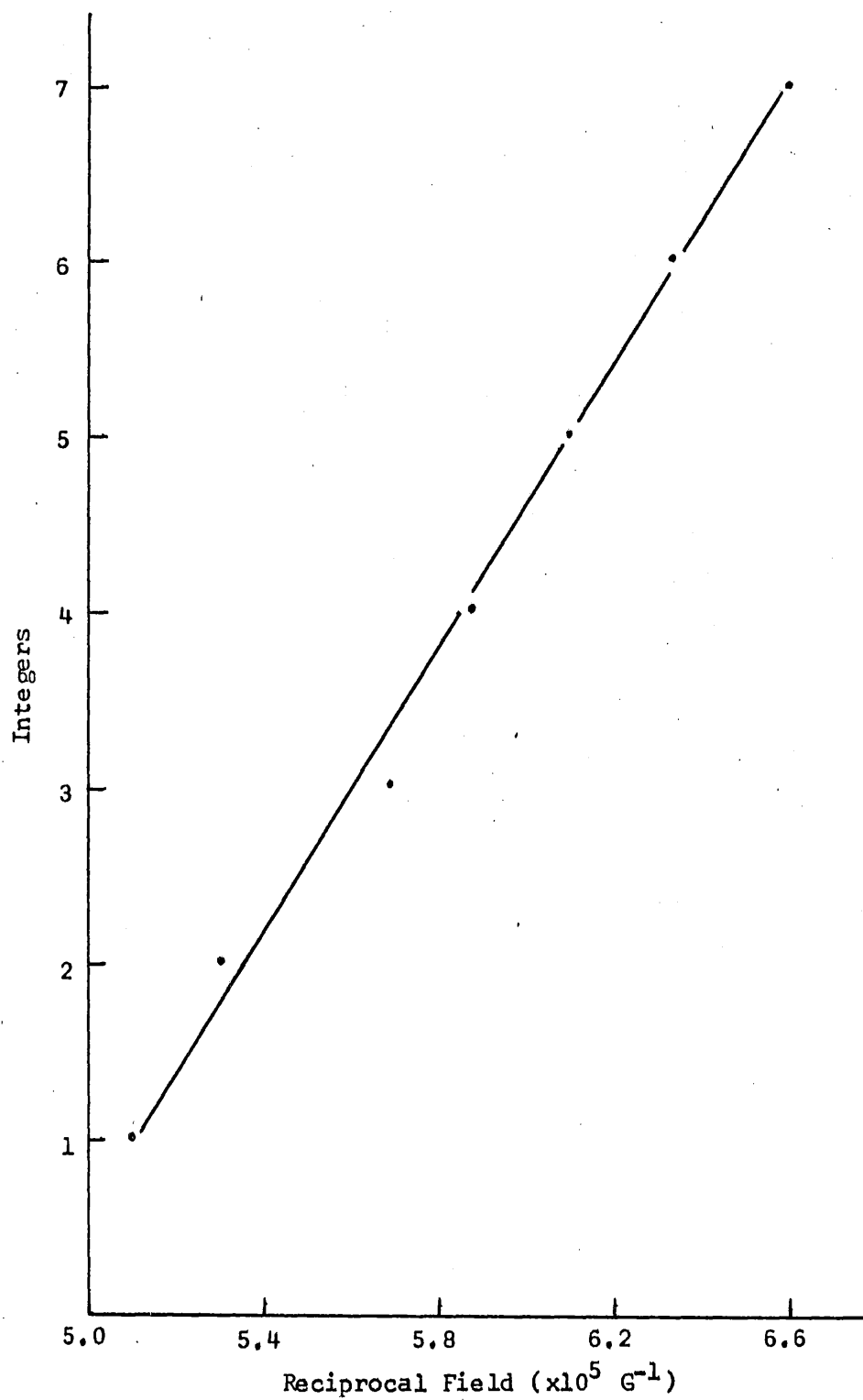


Fig. 12. dHvA Period for Oscillations in FET-ETM-111 Current

experiment, the Kovar-to-glass seal fractured and was repaired. Data were taken, but the seal fractured again. This time it was removed and aluminum foil again used as a guard ring. Data taken subsequently did not indicate that the Kovar guard ring was any more effective than that made by wrapping a portion of the exterior tube wall with foil. Thus, the final two tubes in this project were made with foil guard rings, but of design (B) rather than (A).

With the tube in place in the cryostat and immersed in liquid helium, emission current-voltage data were recorded. The results are illustrated in the Fowler-Nordheim plot in Fig. 13.

A rotation diagram was made after a small, steady field emission current was established. This is illustrated in Fig. 14. Again, the curve is not symmetric in the place of the axis of the field emitter. Reproducibility was more difficult with this tube than with FET-ETM-111, although the general shape of the curve remained the same. The data are not reproduced here.

Experimental Tube FET-ETM-113

This tube was constructed as shown in Fig. 4(B) except that an aluminum foil guard ring was used and the anode was replaced by a tungsten field emitter. The tungsten emitter was formed from a short length of 0.015" tungsten wire. The wire was first beaded with uranium glass and cleaned of oxides in a solution of sodium hypochlorite. The wire was then bent, on a gentle radius, through 90°.

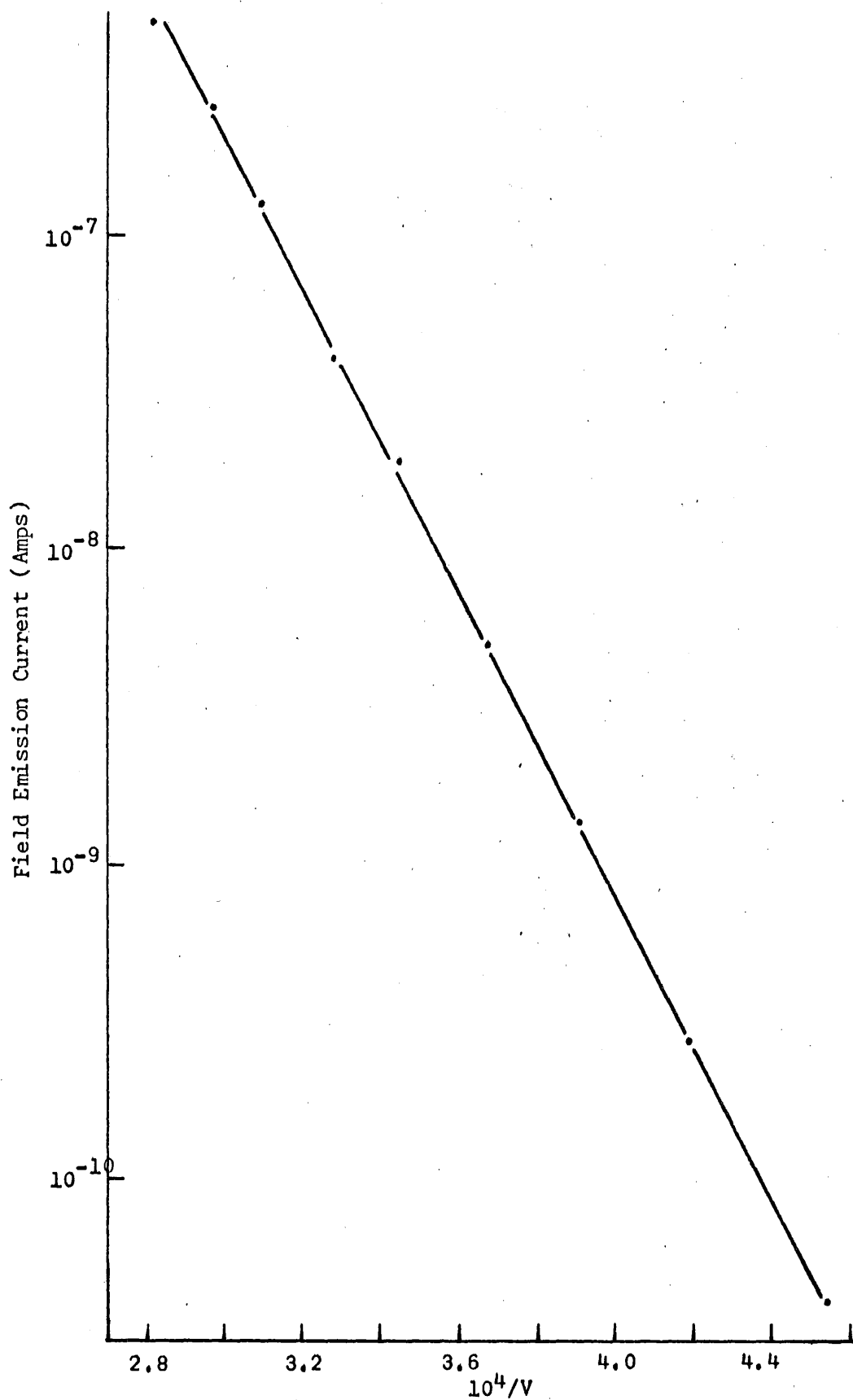


Fig. 13. Fowler-Nordheim Plot for FET-ETM-112

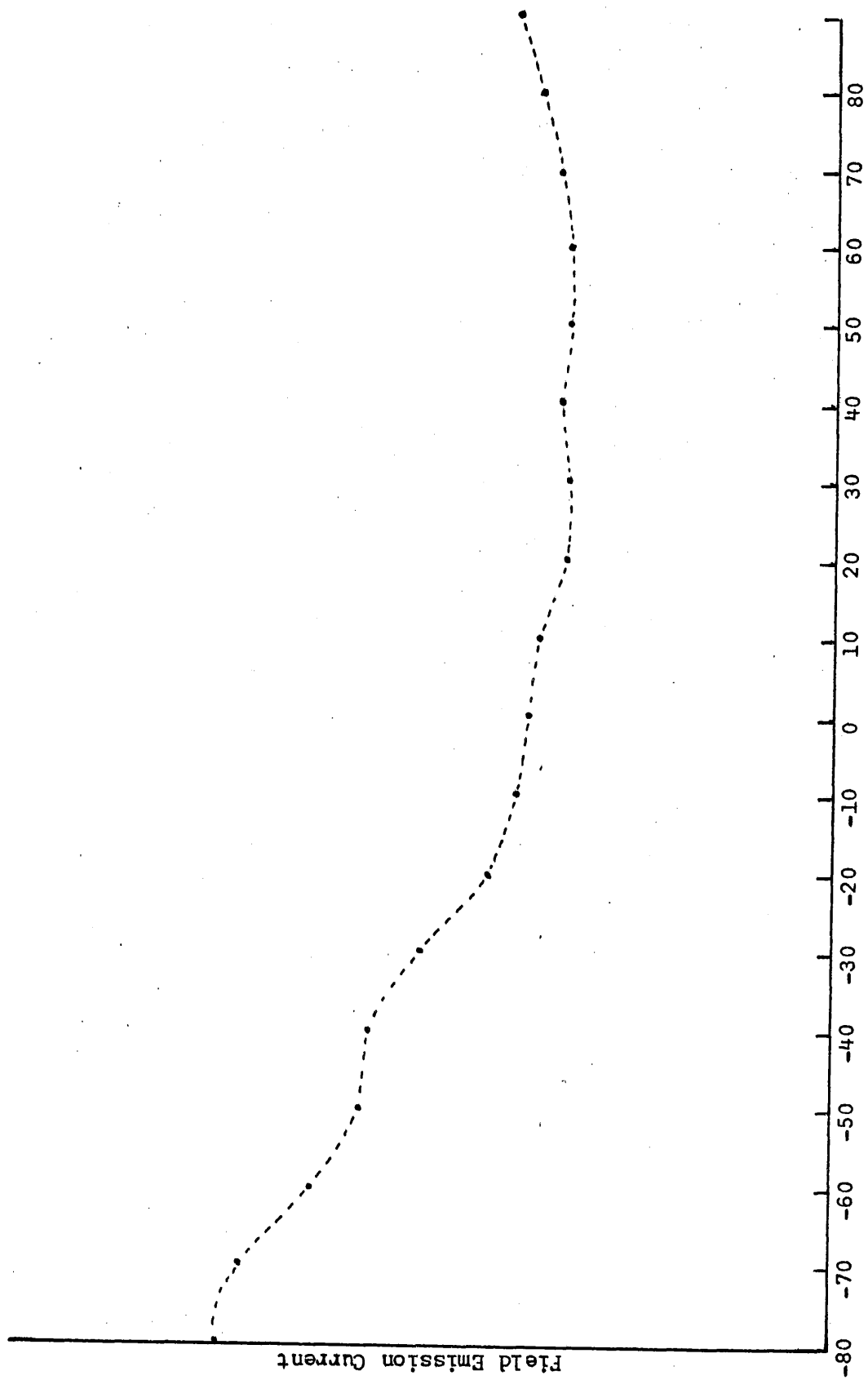


Fig. 14. Rotation Diagram for FET-ETM-112

This end of the wire was electropolished and then etched to a fine point. When the tungsten emitter and bismuth emitters were installed in the field emission tube, they were positioned so that the tips were separated by about one to two millimeters and the emitters were uni-axial. It was felt that two ends could be achieved by this arrangement: (1) the bismuth emitter could be cleaned by electron bombardment from the tungsten emitter, and (2) field emission from tungsten in the presence of a magnetic field could be compared with emission from bismuth under identical environmental conditions. The bismuth emitter was destroyed, however, by serving as an anode for the tungsten emitter, before the electron-bombardment cleaning process could be tried. Nevertheless, it appears that this would be a good technique for cleaning bismuth emitters under the proper operating conditions.

With the tube in place in the cryostat and cooled to liquid helium temperature, I-V data were taken. These are recorded in Fig. 15. It is evident that the emission is field emission.

A rotation diagram is illustrated in Fig. 16. This was taken for a magnetic field of 10 kG. The asymmetry of the rotation curve is very pronounced in this tube. In fact, the emission was extinguished by rotating the magnetic field through 90° . Retrace of the rotation pattern back through 90° did not cause the current to increase. Thus, it appears that the reduction in the size of the anode from one which shielded the emitter from the glass walls to this anode (the tungsten field emitter) had caused electron optical and charging effects to

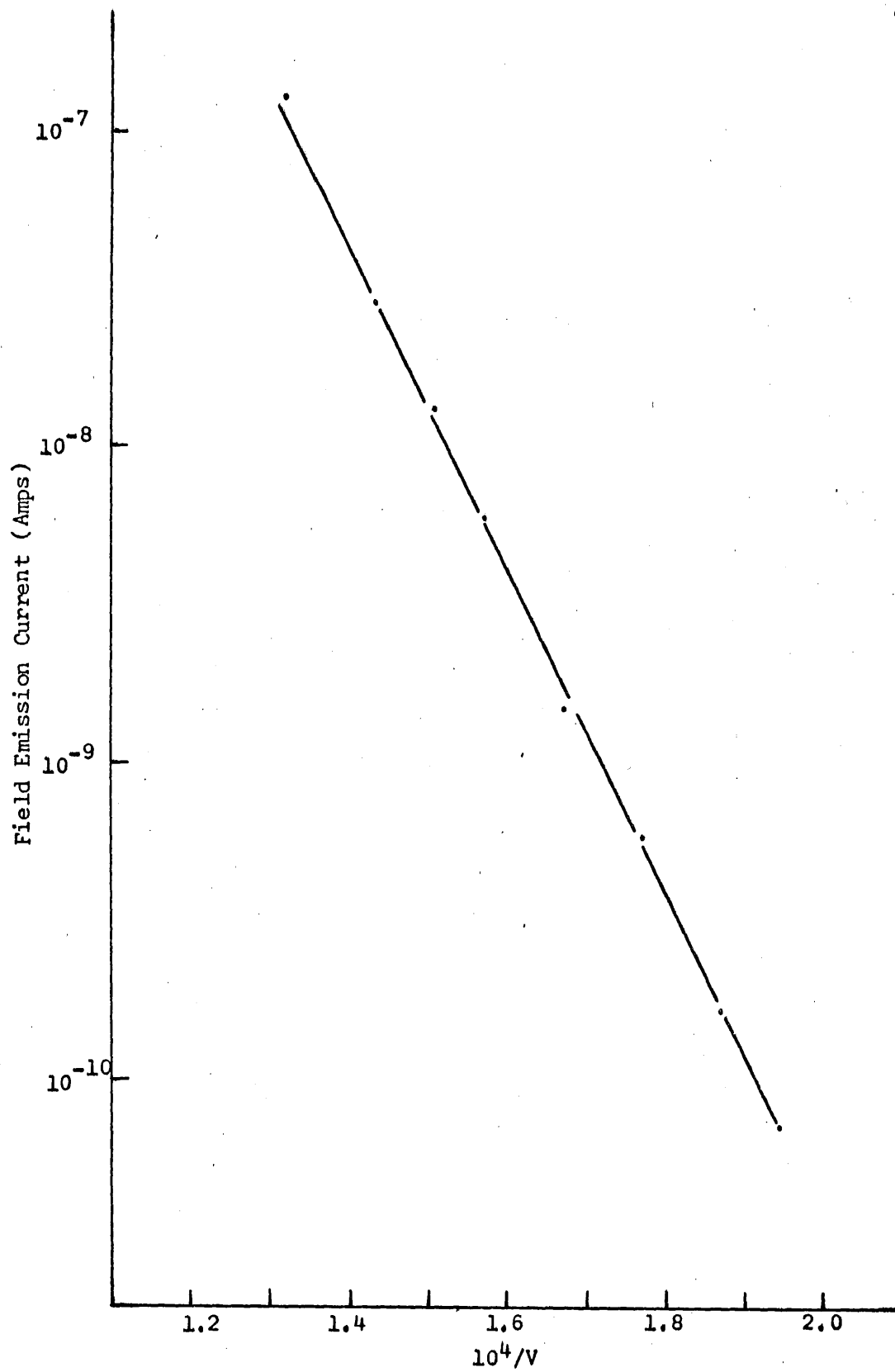


Fig. 15. Fowler-Nordheim Plot for FET-ETM-113

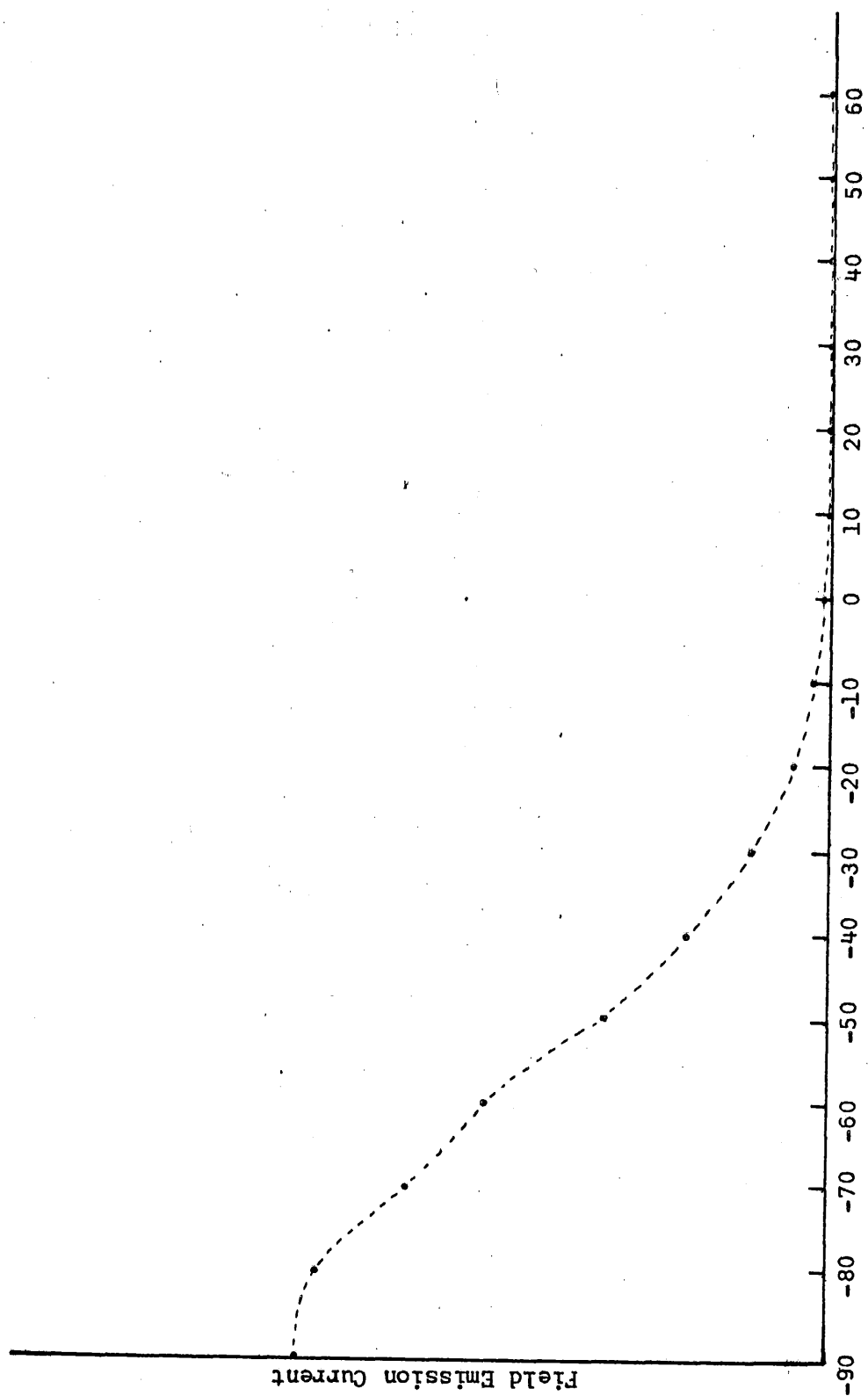


Fig. 16. Rotation Diagram for FET-ETM-113

become very pronounced.

With an initial steady current of 5 nA, the magnetic field was swept to 20.4 kG in 2.5 minutes with the magnetic field parallel to the axis of the emitter. This information is displayed in Fig. 17. No oscillations of the dHvA type are evident. The hump in the curve at low magnetic field intensity is reproducible and probably an electron optical effect. The lower curve is the retrace (B decreasing) of the sweep. The effect of glass charging is evident in the hysteresis effect.

In Fig. 18 is shown the emission from the tungsten emitter and the bismuth emitter (slightly displaced) for initial currents of about 2 nA and with the magnetic field inclined at 40° to the axis of the emitters. The features present in the bismuth emitter curve are also present in the curve for tungsten. No oscillation is evident in either curve at the high field end. The humps in the initial slope occur at the same place in each curve, although it is very doubtful that the geometries of the emitters are close enough to produce identical size-effect oscillations. Thus, it is most probable that these are electron optical effects and that similar anomalies in previous data are also due to electron optical effects rather than a size effect.

Experimental Tube FET-ETM-114

Since much of the structure in the data to this point was thought to be attributable to electron optical effects, and since these seemed

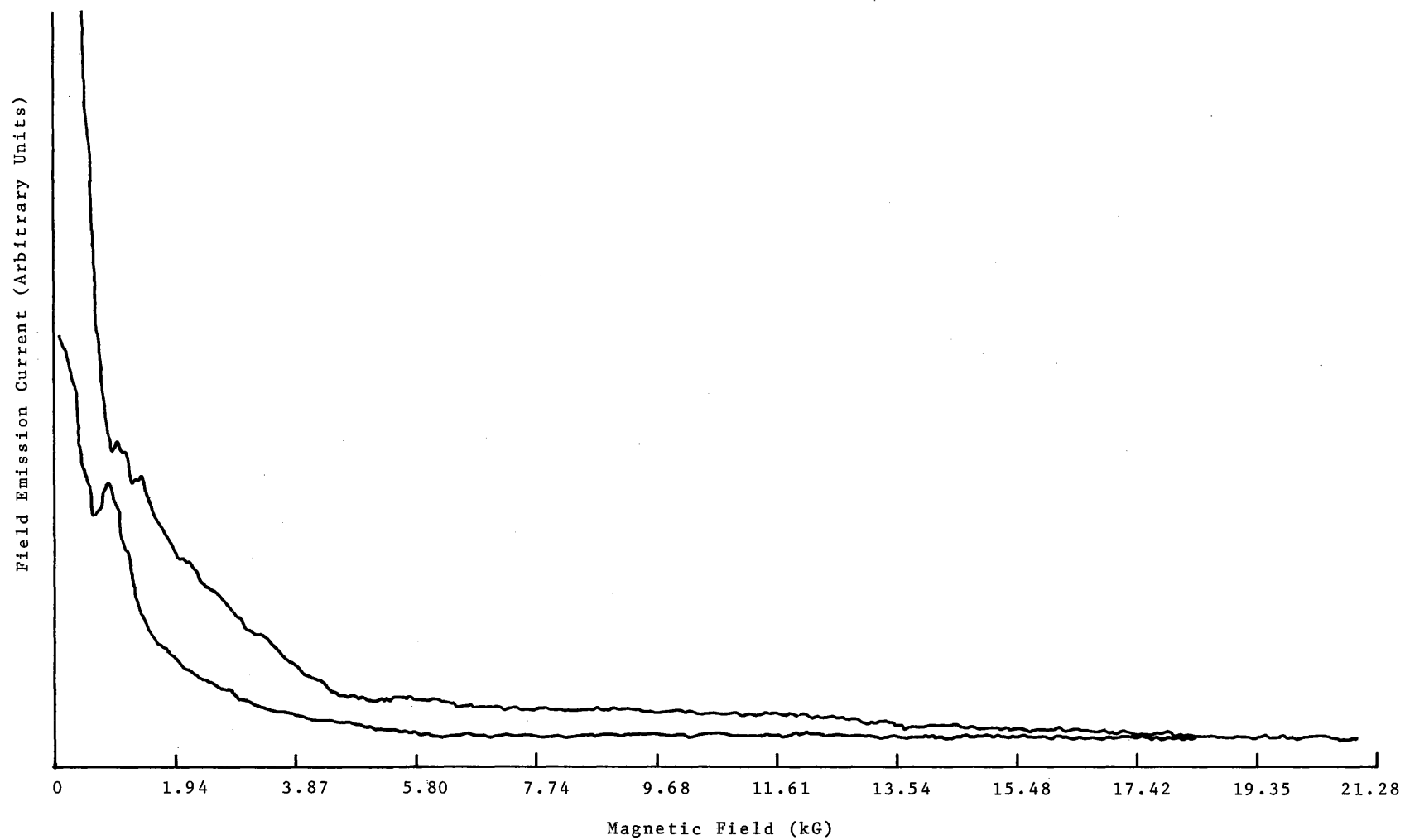


Fig. 17. Magnetic Field Sweep at 0° for FET-ETM-113

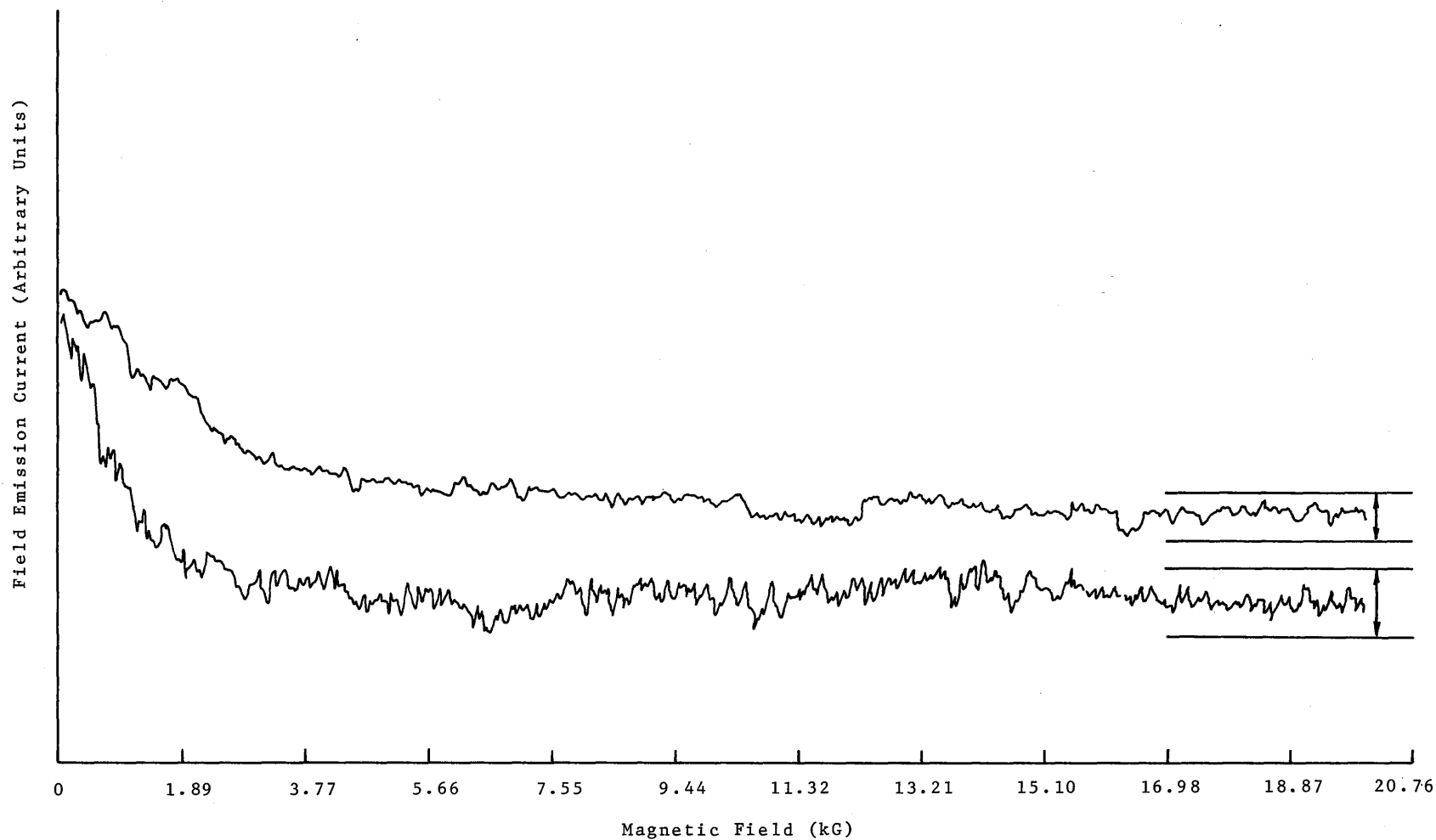


Fig. 18. Field Emission from Tungsten and Bismuth Compared

to be more pronounced as the size of the anode was reduced, this tube was modified by applying a conductive tin oxide coating to the glass wall of the tube envelope in the vicinity of the emitter. This coating was electrically connected to a tungsten field emitter in the same tube and having the same geometry with respect to the bismuth emitter as has been described previously. The tube envelope was of the same design as that of FET-ETM-113. An aluminum foil guard ring was used.

Field emission current was first obtained at 800 volts and was exceptionally steady. The I-V characteristic was taken and is illustrated in Fig. 19. It is clearly Fowler-Nordheim (See previous discussion of criteria for field emission, p. 30).

With a small current being drawn from the bismuth, the magnetic field was rotated as in previous experiments. This had no effect on the magnitude of the field emission current within the limits of our measurement. This result tends to confirm the previous hypothesis that variations in field emission current with magnetic field rotation were due to electron optical and not solid state anisotropic effects. In the light of the results obtained from FET-ETM-111, however, the rotation should be more carefully investigated.

Field emission current dependence was measured for several orientations of the magnetic field with respect to the axis of the emitter and at several different initial currents (Fig. 20). It sometimes appeared that oscillations began to occur at the high end of the magnetic field, though they never seemed to change amplitude with increasing magnetic field as one would expect of a dHvA type

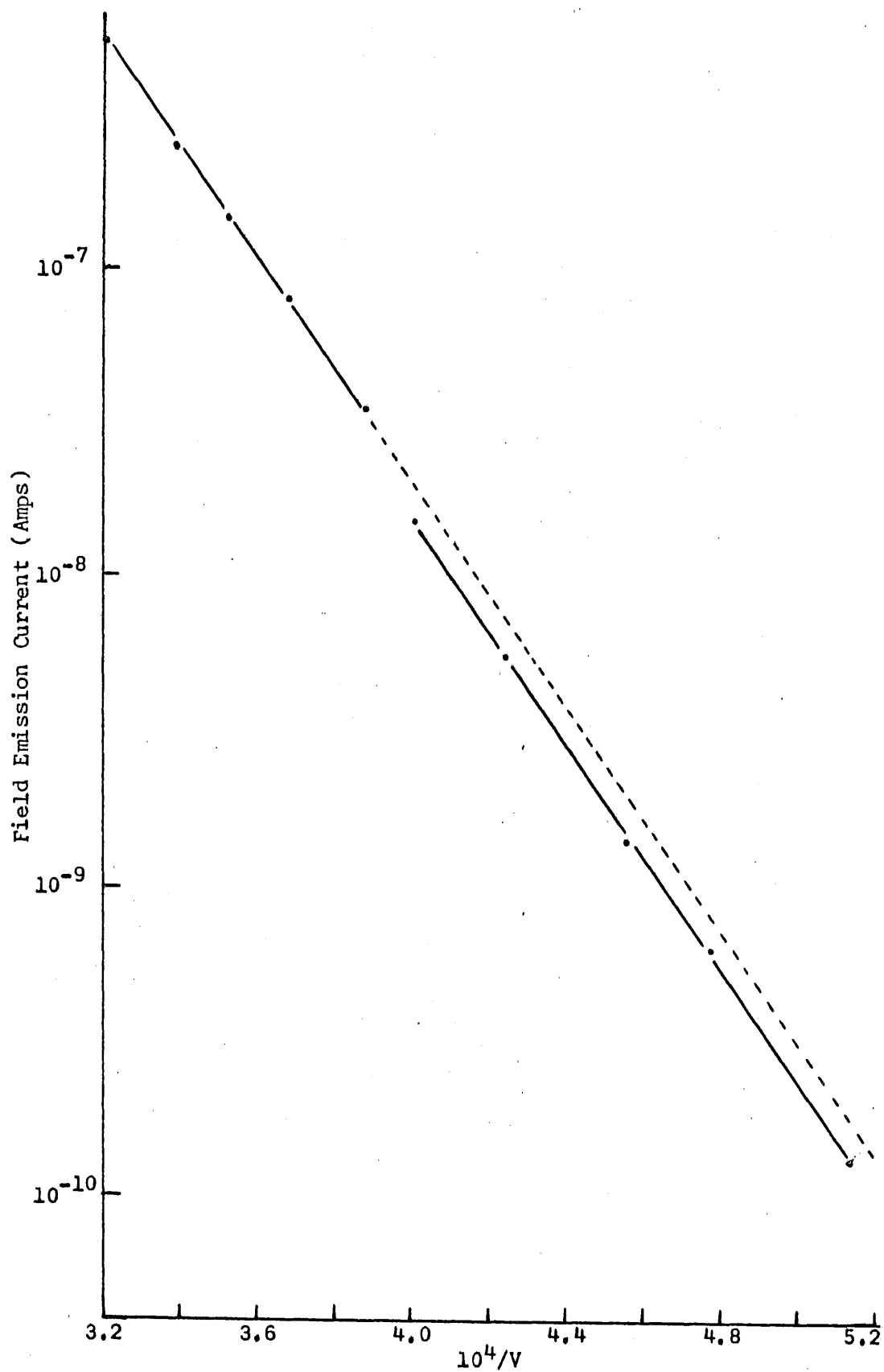


Fig. 19. Fowler-Nordheim Plot for FET-ETM-114

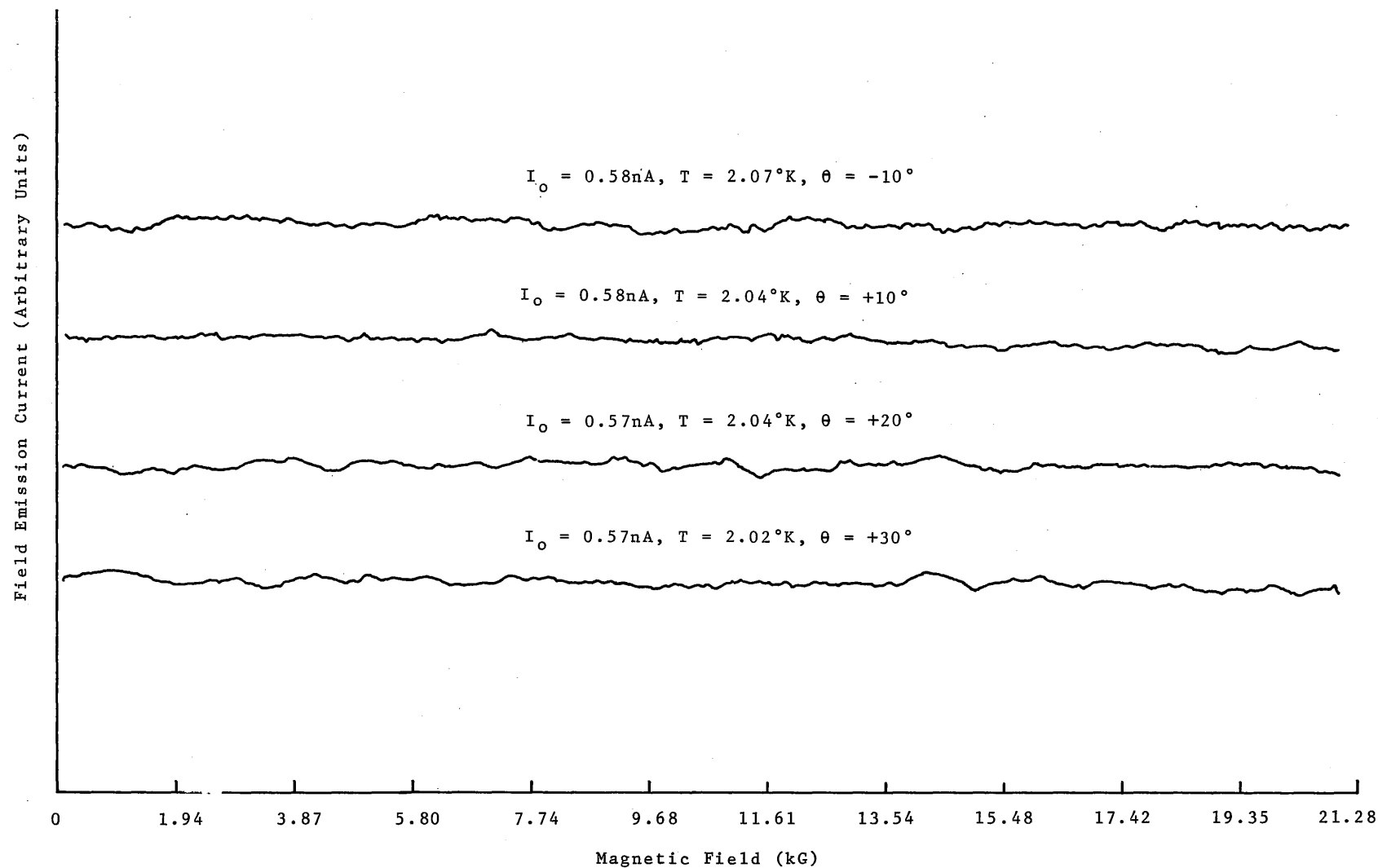


Fig. 20. Magnetic Field Sweep Below λ -Point for FET-ETM-114

oscillation and they were not reproducible; therefore, they are attributed to small random fluctuations in the field emission current. Since it was felt that random temperature fluctuations might be causing dHvA oscillations to be obscured, the temperature was brought below the λ -point for these measurements. There was a definite improvement in the stability of the signal, but the dHvA effect was, nevertheless, not observed even at 2.02°K.

Discussion

The phenomenon of field emission has been investigated experimentally in the temperature range 2.02°K to 4.2°K and in magnetic fields up to 20.4 kG for field emitters fabricated from capillary crystals of bismuth. A search has been made for quantum oscillations of the dHvA type. In the best experiments, performed with FET-ETM-114, the noise level was significantly below that which would be required to observe the dHvA effect at the level predicted by the theory of Blatt. In most of the experimental data, dHvA-like oscillations have not been observed. In the data reported for FET-ETM-111, however, oscillations of the dHvA type may be present. The oscillations present in those data were found to be periodic in B^{-1} with a period corresponding to that which has been reported² for the single hole ellipsoid of bismuth in an axis normal to the trigonal axis. Since the crystallographic orientation of the sample used in these experiments is unknown, however, it is impossible to positively confirm the fact that the dHvA effect was observed in field emission current.

Since quantum oscillations were not observed in most of the experimental data, it is important to consider some of the possible causes for the essentially null result of this work.

Assumptions of the Analysis of Blatt's Theory

The results of the theory by Blatt suggest the presence of quantum oscillations in field emission currents (Appendix A and Fig. 1). In the development of the theory, it was assumed that: (1) the tunneling probability for field emitted current was explicitly independent of the magnetic field strength; (2) the analysis was valid in the zero-temperature limit; and (3) that realistic results were obtainable using a quasi-free electron model.

According to Blatt, assumption (1) could not be justified by recourse to either theoretical or experimental information since neither was available at the time of the writing of the article (1963). To this author's knowledge, this is still the case. If the penetration probability were in fact an explicit function of the magnetic field strength, one might very well expect that the results of Blatt's analysis would be modified.

Blatt's theory and numerical analysis are valid in the limit of zero degrees. Experimental observation of the dHvA effect must, of course, be made at some temperature above zero degrees. It is important, therefore, to consider the possible effect on the amplitude of the oscillations predicted by Blatt as a result of having to work at temperatures above zero degrees. In our experimental search for quantum oscillations, the lowest temperature attained was 2.02°K, although with only slightly more effort the temperature could probably have been reduced another few tenths of a degree. In its simplest

form, the amplitude of the dHvA oscillations is expressed in terms of the field and temperature by the term³⁴

$$\exp[-2\pi^2 k_B (T + T') / \beta H] \quad [2]$$

where T is the temperature of the sample, T' is the Dingle temperature (to be discussed below), $\beta = e\hbar/mc$ (the double Bohr magneton for a free electron), k_B is Boltzmann's constant and H is the magnetic field intensity. The assumption made in the theory by Blatt is that this term is unity [$(T + T') = 0$]. Making the assumption that $T = 1^\circ\text{K}$ and $T' = 0$, very good conditions indeed, one finds that the value of the term in brackets is fifteen for m equal to the free electron mass and a field of 10 kG. The amplitude of the dHvA effect under these conditions would certainly prevent their measurement in this experiment, but the value calculated above is quite pessimistic. Using the value $m = 0.0105m_0$ quoted by Blatt would reduce the exponential term to $e^{-0.15} = 0.86$. Thus, if a temperature of $T = 1^\circ\text{K}$ were obtainable for these measurements, one would expect the amplitude of the oscillations to be only slightly less than was predicted by Blatt. On the other hand, our observed temperature was 2.02°K in the best experiments and usually 4.2°K . Thus, on the basis of the bath temperature alone, one would expect the magnitude of the oscillations to be about 0.74 and 0.55 of that predicted by Blatt at 2°K and 4.2°K , respectively. If the amplitude of the oscillations predicted by Blatt had been reduced by these amounts, the oscillations could have been detected with the sensitivity of our experiments.

The final assumption made in Blatt's analysis was that the Fermi surface was spherical. It is well known, however, that the Fermi surface of bismuth is far from spherical.²² According to Kao,²⁴ the effective mass of holes ranges from $0.067m_0$ to $0.226m_0$ as the magnetic field is swung from a position parallel to the trigonal axis to a position normal to the trigonal axis. The effective masses for electrons in the binary, bisectrix and trigonal axes are: 0.0107, 0.14; 0.0091, 0.0196; and 0.081, respectively. Thus, if the temperature is assumed to be 4,2°K ($T' = 0$) and it is assumed that the axis of the emitter is along the trigonal axis, then oscillations of a magnitude of 0.01 times that predicted by Blatt would be expected. This is clearly well beyond the sensitivity of the present experiment. If, however, the field emitter were grown along a binary axis, one would expect to see oscillations of about half the amplitude predicted by Blatt. Finally, with the emitter grown along a bisectrix axis, one might expect to find oscillations from two parts of the Fermi surface, one oscillatory component having an amplitude of 3% of the total signal and the other having an amplitude of about 5% (one half of Blatt's predicted amplitude) of the total signal. The periods of the two oscillations would differ by a factor of two.

Thus, it appears that even under the best conditions available during this work, the amplitude would have been reduced by a small amount from the amplitude predicted by Blatt. If the emitter had grown along the trigonal axis, or an axis near the trigonal axis, it is doubtful that oscillations could have been detected at all.

In all of the foregoing, it has been assumed that $T' = 0$. T' is an effective temperature introduced by Dingle¹¹ to account for collision broadening of the Landau levels and consequent reduction in the amplitude of the dHvA effect. The Dingle temperature is usually on the order of 1°K and is nearly isotropic for large crystals. The Dingle temperature is given by

$$T' = \hbar / \pi k_B \tau \quad [3]$$

where τ is a characteristic relaxation time, the mean time between collisions of a carrier. In a field emitter of a material such as bismuth with a non-spherical Fermi surface, τ is anisotropic. If l is taken to be the mean free path of the carrier and v_f the Fermi velocity, then τ is given by

$$\tau = l / v_f$$

In the worst case, l is arbitrarily limited by the diameter of the field emitter and is therefore on the order of 10^{-4} cm or less. Taking v_f to be given by $\hbar k / m^*$, the expression for T' becomes

$$T' = \hbar^2 / \pi k_B l \quad (k / m^*) \quad [4]$$

When this term is included in [2], the expression for the amplitude of the dHvA oscillations becomes

$$\exp[-(hc/e l H) \bar{k}] \exp[-(2 \pi^2 k_B T / \beta H)] \quad [5]$$

We have just dealt with the last exponential in this expression. It

remains to be seen what effect on the amplitude is produced by the first exponential. Assuming $\ell = 10^{-4}$ cm, [5] becomes

$$\exp[-4.85 \times 10^{-7} \vec{k}] \exp[-(2 \pi^2 k_B T / \beta H)] \quad [6]$$

It is now clear that, under the usual experimental conditions attained in this work ($T = 4.2^\circ\text{K}$), the contribution of the Dingle temperature term could have made the observation of the dHvA effect nearly impossible. The values of k have been calculated in Appendix C in the electron ellipsoidal axes. It has been shown already that, if the emitter were grown along the trigonal axis, the amplitude of the dHvA effect would be expected to be on the order of 0.1% of the total signal and not 10% as predicted by the analysis of Blatt. The Dingle temperature term would tend to lower this estimate. For a growth of the emitter along a binary axis, we have anticipated a dHvA amplitude of about 5% of the total signal and the period of this should be about $7.2 \times 10^{-5} \text{ G}^{-1}$. The Dingle temperature term would tend to decrease this estimate considerably since the effective value of k_{max} is $6.22 \times 10^5 \text{ cm}^{-1}$. The contribution from the first exponential in [6] would then be 0.73 and the amplitude of the dHvA effect would be expected to be of the order of 3.7% of the total field emission current. Finally, if the emitter were grown along a bisectrix axis, we have found that one might expect to see two oscillatory components in the dHvA oscillations, one of which would be on the order of 5% of the total signal and having a period of approximately $8.3 \times 10^{-5} \text{ G}^{-1}$ while the other would have an amplitude of about 3% and a period of

approximately $4.17 \times 10^{-5} \text{ G}^{-1}$. Inclusion of the Dingle temperature term would cause the 5% magnitude to be reduced to 3.6% and the 3% contribution to be reduced to about 2.5% of the total signal.

In summary of the above analysis, it has been shown that, with a bath temperature of 4.2°K and the appropriate collision broadening contribution to the reduction in the amplitude of the dHvA effect, dHvA-like oscillations in field emission current could be expected to have an amplitude of less than 1% for field emitters prepared from bismuth which were grown on the trigonal axis. For an emitter grown on a bisectrix or binary axis, the amplitudes to be expected are on the order of 3% to 4% of the total signal. Lowering the temperature to 2.02°K would increase the amplitudes. Given that the noise level of this experiment ranged from 3% to 5% of the total signal, it is not surprising that dHvA oscillations were not observed in most of this work. For FET-ETM-111, the period measured was $0.50 \times 10^{-5} \text{ G}^{-1}$. Yet, with the sensitivity of this experiment, we would only have expected to measure periods of 4.17×10^{-5} , 8.3×10^{-5} , and $7.2 \times 10^{-5} \text{ G}^{-1}$. It is not likely that we would have seen oscillations from the hole ellipsoid with the crystal grown on a bisectrix or binary axis because of the large effective hole mass in this direction.

One final point should be mentioned with respect to thermal lowering of the amplitude of the dHvA effect in field emitters. It might be thought that Joule heating and other heating mechanisms would cause the emitter temperature to rise during field emission. It has been shown (Appendix B) that these effects are very small for all

of the work performed here and thus the major thermal problems arise from high bath temperature and an anisotropic Dingle temperature.

Field Emitters and Fermi Surfaces

It is important to mention two more problems which, although not explicitly considered in Blatt's analysis of the theory, are nevertheless implicit assumptions of the analysis.

In large samples, one need not usually be concerned about the breakdown of the quantized Landau levels due to collisions of carriers with the walls of the sample. In a sample of the size of a field emitter, however, this might well be a problem. Since the Fermi surface is not spherical (See Appendix C for a description of the FS of bismuth), the radii of quantized orbits will vary, for a given value of the magnetic field strength, with the crystallographic direction of growth of the emitter. It has been shown in Appendix C that the optimal growth direction is along the bisectrix axis where, at 10 kG, the radii would be expected to be of the order of 450\AA . Field emission can be attained at reasonably low voltages (2000 volts) with emitters having a radius of 1000\AA , and thus, size effects would not constitute a problem. For emitters grown along a binary axis, the radius of a maximum orbit at 10 kG has been shown to be 5600\AA . Thus, if the emitter were grown along a binary axis, the radius of the emitter would have to be larger than 5600\AA and voltages on the order of 8000 volts would be required.

It was mentioned in Chapter I that the dHvA effect might be a very good tool by which the Fermi surface could be studied near real surfaces. It has been tacitly assumed, both by Blatt and the present author, during the course of discussion that the Fermi surface concept is still good for small samples in the presence of very high electric fields. This assumption is by no means trivial. If the FS were considerably modified by the high field at the surface of the emitter, then it would be difficult to compare the oscillatory periods of the dHvA effect observed in field emission current with the periods usually observed in larger samples which are not subjected to such high fields. It is known, for example, that the lattice of a field emitter can be expanded by the "negative hydrostatic pressure" of the high field in field ion microscopy. This would certainly change the Brillouin zone dimensions and affect the Fermi surface. On the other hand, localized stress at the surface of the sample (e.g. surface tension) might also cause the Fermi surface to be modified. If the discovery of the dHvA effect were to be confirmed in field emission current, the technique of observing the dHvA oscillations in field emission current for several values of electric field strength might well shed light on the concept of Fermi surfaces near real surfaces.

Conclusions and Recommendations

Conclusions

Field emission from bismuth has been investigated at low temperatures in magnetic fields up to 20.4 kG. A search was made for de Haas-van Alphen-like quantum oscillations in the emitted current. With the exception of one experiment, no oscillations appeared in the field emission which could be identified as dHvA oscillations. A review of the assumptions made by Blatt for the numerical analysis of his theory suggested that, under the conditions of the experimental work reported herein, oscillations would not have been expected to appear except in the case of an emitter grown normal to the trigonal axis. In addition, it was found that even under the best conditions presently attainable, the effect will, for most crystallographic orientations of the emitter axis, be much smaller than was predicted by Blatt. Finally, even if the effect were to be observed in field emission current, one would not necessarily expect the periods of the dHvA oscillations to correspond to the periods found in larger samples of the same crystallographic orientation.

Recommendations for Further Work

The results of this work suggest that considerably more experimental sophistication than was used here will be required for

the observation of the dHvA effect in field emission current.

The most obvious recommendation is, of course, that the field emission tube FET-ETM-111 be retested in order to confirm the observation of the dHvA effect reported in this thesis. In future work, it is recommended that field emitters be prepared from crystals grown on a bisectrix axis. Thus, it will probably not be possible to use the growth techniques used in this work. A "soft-mold" method would be preferred in which the growth could be seeded. The mold could probably be prepared from pyrex glass tubing with an inner bore of 3 mm and cut in half along the axis. The rough single crystal could be smoothed in HNO_3 and etched chemically or electrolytically.

The tube design used in this work was especially suitable for the geometry of the Dewar and magnet. Especially suitable was the use of a reentrant (Dewar) seal, which permitted more direct contact of the helium bath to the crystal. If it were possible to make the tube axially symmetric, however, by the use of a superconducting solenoid to develop the magnetic field, this would be preferable. This would allow more room in the tube so that larger crystals could be used. It would also allow enough room to include a detachable crystal holder in the tube so that the crystal could be examined under an electron microscope to determine the emitter radius, and under X-ray diffraction to determine the crystallographic orientation. Both of these analyses will be required for quantitative analysis of the dHvA effect in field emission. The geometry of the system used in this work prevented the incorporation of X-ray and electron microscopic evaluation of the

emitter used for field emission measurements.

Since it is anticipated that the dHvA effect will be more nearly on the order of 0.1% to 4% than the previously predicted level of 10% for most orientations, it will not be possible to use the same electronic system as was used in this work. In the last few experiments, a Sola regulator was incorporated in the A.C. line of the high voltage supply. Although this reduced the noise somewhat, it will probably be necessary to use a well regulated high voltage supply for future work. In addition, lock-in techniques should also be incorporated to segregate noise from the field emission signal. Unless a means is devised by which the emitter can be cleaned, such as was suggested earlier, noise can be expected in the field emission signal due to sub emitters on the main emitter and/or adsorbed species on the emitter.

Bibliography

1. Bhargat, S.M. and Manchon, D.D. (Jr.). "Heat Transport in Bismuth at Liquid-Helium Temperatures," Phys. Rev. 164, 966 (1967).
2. Bhargava, R.N. "de Haas-van Alphen and Galvanomagnetic Effect in Bismuth and Bi-Pb Alloys," Phys. Rev. 156, 785 (1967).
3. Bar'yakhtar, V.G. and Makarov, V.I. "Concerning the Oscillations of the Tunnel Current in a Magnetic Field," Soviet Physics-Doklady (U.S.A.) 146, 63 (1962).
4. Blatt, F.J. "Field Emission in a Magnetic Field," Phys. Rev. 131, 166 (1963).
5. Bridgeman, P.W. Proc. Am. Acad. Arts and Sciences 60, 303 (1925).
6. Burgess, R.E. and Kroemer, H. "Corrected Values of Fowler-Nordheim Field Emission Functions $v(y)$ and $s(y)$," Phys. Rev. 90, 515 (1953).
7. Chynoweth, A.G., et al. "Effect of Landau Levels upon Tunnel Currents in Indium Antimonide," Phys. Rev. Letters 5, 548 (1960).
8. Cooper, E.C. "Field Desorption by Alternating Fields. An Improved Technique for Field Emission Microscopy," Rev. Sci. Inst. 29, 309 (1958).
9. de Hass, W.J. and van Alphen, P.M. Communication Phys. Lab., Univ. Leiden, 212 A (1930).
10. de Haas, W.J. and van Alphen, P.M. Communication Phys. Lab. Univ. Leiden, 220 D (1932).
11. Dingle, R.B. "Some Magnetic Properties of Metals. II. The Influence of Collisions on the Magnetic Behavior of Large Systems," Proc. Royal Soc. 211, 517 (1952).
12. Dolan, W.W., et al. "The Field Emission Initiated Vacuum Arc. II. The Resistively Heated Emitter," Phys. Rev. 91, 1054 (1953).
13. Dyke, W.P., et al. "The Field Emitter: Fabrication, Electron Microscopy, and Electric Field Calculations," J. Applied Phys. 24, 570 (1953).

14. Dyke, W.P. and Dolan, W.W. Advances in Electronics and Electron Physics. Vol. VIII. New York: Academic Press Inc., 1956.
15. Fowler, R.H. and Nordheim, L. "Electron Emission in Intense Electric Fields," Proc. Roy. Soc. London A119, 173 (1928).
16. Friedman, A.N. and Koenig, S.H. "Size Effects for Conduction in Thin Bismuth Crystals," I.B.M. Journal, (April 1960).
17. Gogadze, A., et al. "Quantum Oscillations of the Field Emission Current from Metals in a Magnetic Field," Soviet Physics-JETP 19, 622 (1964).
18. Gomer, R. "Field Emission from Mercury Whiskers," J. Chem. Phys. 28, 457 (1958).
19. Gomer, R. Field Emission and Field Ionization. Cambridge: Harvard Univ. Press, 1961.
20. Good, R.H. and Muller, E.W. Handbuch der Physik. Vol. XXI. Berlin: Springer-Verlag, 1956.
21. Horl, E.M. "Image of the Fermi Surface in Field Emission Patterns," Acta. Phys. Austriaca 18, 33 (1964).
22. Jain, A.J. and Koenig, S.H. "Electrons and Holes in Bismuth," Phys. Rev. 127, 442 (1962).
23. Kahn, A.H. and Frederikse, H.P.R. Solid State Physics. Vol. IX. New York: Academic Press, 1959.
24. Kao, Yi-Han. "Cyclotron Resonance Studies of Fermi Surfaces in Bismuth," Phys. Rev. 129, 1122 (1963).
25. Kapitza, P. "The Study of the Specific Resistance of Bismuth Crystals and its Change in Strong Magnetic Fields and Some Allied Problems," Proc. Roy. Soc. London A119, 358 (1928).
26. Kulik, I.O. and Gogadze, G.A. "Quantum Oscillations of the Tunnel Contact Current of Two Metals in a Magnetic Field," Soviet Physics-JETP 17, 361 (1963).
27. Machinnon, L. Experimental Physics at Low Temperatures. Detroit: Wayne State Univ. Press, 1966.
28. Marcus, Jules A. Phys. Rev. 71, 559 (1947).
29. Marcus, Jules A. "Temperature Dependence of Susceptibility of Zinc, Cadmium, and Gamma-Brass," Phys. Rev. 76, 621 (1949).

30. Mayer, L. et al. "Bismuth Whisker Growth," J. Applied Phys. 33, 982 (1962).
31. Melmed, A.J. and Gomer, R. "Field Emission from Whiskers," J. Chem. Phys. 34, 1802 (1961).
32. Nordheim, L. "The Effect of the Image Force on the Emission and Reflection of Electrons by Metals," Proc. Roy. Soc. London A121, 626 (1928).
33. Schoenberg, A. "The de Haas-van Alphen Effect," Phil. Trans. Roy. Soc. A891, 245 (1952).
34. Schoenberg, D. Low Temperature Physics LT 9. New York: Plenum Press, 1965.
35. White, G.K. and Woods, S.B. "The Thermal and Electrical Resistivity of Bismuth and Antimony at Low Temperatures," Phil Mag. 3, 342 (1958).
36. Ziman, J.M. Electrons in Metals: A Short Guide to the Fermi Surface. London: Taylor and Francis Ltd., 1963.

Appendix

Appendix A

Elements of Field Emission Theory

It has been found that electrons can be emitted from cool metallic surfaces in the presence of strong electric fields. This phenomenon is called field emission. Unlike thermionically emitted electrons which must gain enough energy to pass over a surface potential barrier, field emitted electrons penetrate the barrier by a quantum process called "tunneling."

The surface barrier is illustrated in Fig. 1(A). Its composition is threefold: (1) inside the metal, the potential energy has some constant value, $-\phi_a$, with respect to a zero level when the electron and metal are separated; (2) outside the metal, in a one-dimensional representation, the applied electric field contributes a potential term, $-eEz$; (3) also outside the metal, the electron is attracted to the surface by the charge it induces there. This energy of position is referred to as an image potential. Increasing the electric field strength causes the barrier to be lowered, thinned, and moved closer to the surface.

If $N(W)d(W)$ is the electron flux per second, with z -component of energy within dW , incident on the surface barrier from within the metal, and $D(W)$ is the probability of penetration of the barrier, then the product of these two terms gives the electron flux per second emerging from the metal. The emitted current density is then

$$J = -e \int_{-\phi_a}^{\infty} N(W)D(W)dW \quad [A.1]$$

It has been shown that $N(W)$ and $D(W)$ are of the form²⁰

$$N(W) = (4\pi mkT/h^3) \ln[1 + \exp(\mu - W)/kT] \quad [A.2]$$

$$D(W) = \exp[[-4(2m|W|^3)^{1/2}/3e\hbar E] \xi(y)] \quad [A.3]$$

where E is the electric field strength, μ is the Fermi energy and $\xi(y)$ is a term of the order of unity. When these forms for $N(W)$ and $D(W)$ are used to evaluate the integral in [A.1], the following expression for the current density of field emitted electrons results

$$J = A'E^2 \exp(-B'/E) \quad [A.4]$$

with $A' = 1.54 \times 10^{-6} / \phi t^2(y)$

$$B' = 6.83 \times 10^7 \phi^{3/2} \xi(y)$$

where ϕ is the work function of the metal. $t(y)$ and $\xi(y)$ are tabulated functions.⁶ Equation [A.4] is the Fowler-Nordheim equation. A plot of $\ln J/E^2$ versus $1/E$ which is linear over several orders of magnitude is usually taken to be a sufficient condition for field emission.

In the foregoing, it was assumed that the field emission was unperturbed by the presence of a magnetic field. In an extension of the theory of field emission, Blatt⁴ considered the effect of a quantizing magnetic field on the field emission current. The theory was formulated in the limit of zero degrees for a free electron gas

model. It was also assumed that $D(W)$ is not an explicit function of the magnetic field strength.

In the presence of a magnetic field directed along the z -axis, the momentum p_z is unaffected, but quantized orbits are formed in the plane normal to z , with allowed energy levels

$$W + E_n = (\hbar^2/2m^*)k_z^2 + (n + 1/2)\hbar\omega \quad [A.5]$$

where ω is the cyclotron frequency, n is an integer greater than or equal to zero and \hbar is Planck's constant divided by 2π . The density of states function with constant n is

$$N_n(E) = (2eH/h^2c)(2m^*)^{1/2}(E - E_n)^{-1/2} \quad [A.6]$$

As before, we are interested in determining the flux of electrons at the surface in the range between W and $W + dW$. In terms of the total energy, this is $1/2 f(E) v_{z,n}(E) N_n(E) dE$, where $f(E)$ is the Fermi distribution function and the one-half arises on account of the fact that only one half of the electrons traveling in the z -axis are moving toward the surface. The field emission current is then found in a manner similar to that suggested in [A.1], except that the expression must be summed over all orbital quantum numbers. Thus,

$$J = A \sum_n B_n \int_{E_n}^{\infty} f(E) e^{E/d} dE \quad [A.7]$$

with A, B_n, g and d defined as follows below.

$$A = (2e^2 H / h^2 c) \exp[-(g + \eta/d)]$$

$$B_n = \exp[-E_n/d]$$

$$g = [6.83 \times 10^7 \phi^{3/2}/F] \xi(y)$$

$$d = 9.76 \times 10^{-9} F / [(m^*/m)^{1/2} \phi^{1/2} t(y)]$$

When the summation indicated in [A.7] is performed in the limit of $T \rightarrow 0$, the following result, due to Blatt, is obtained.

$$J = Ad[(d(e^{\eta/d} - 1) - \eta)/\hbar\omega + \sum (-1)^p \{ [2/(4\pi^2 p^2 + (\hbar\omega/d)^2)] \\ \times [2\pi p \sin(2\pi p \eta/\hbar\omega) - (\hbar\omega/d)(\cos(2\pi p \eta/\hbar\omega) - e^{\eta/d})] \\ - (1/\pi p) \sin(2\pi p \eta/\hbar\omega) \}] \quad [A.8]$$

Equation [A.8] is the final expression for field emission current in a magnetic field. A numerical analysis of this expression was carried out on an IBM 1130 system. The results of this analysis appear in Fig. 1. Oscillations of the dHvA type are predicted in the field emission current which have an amplitude of about ten per cent of the average signal above ten kilogauss for bismuth.

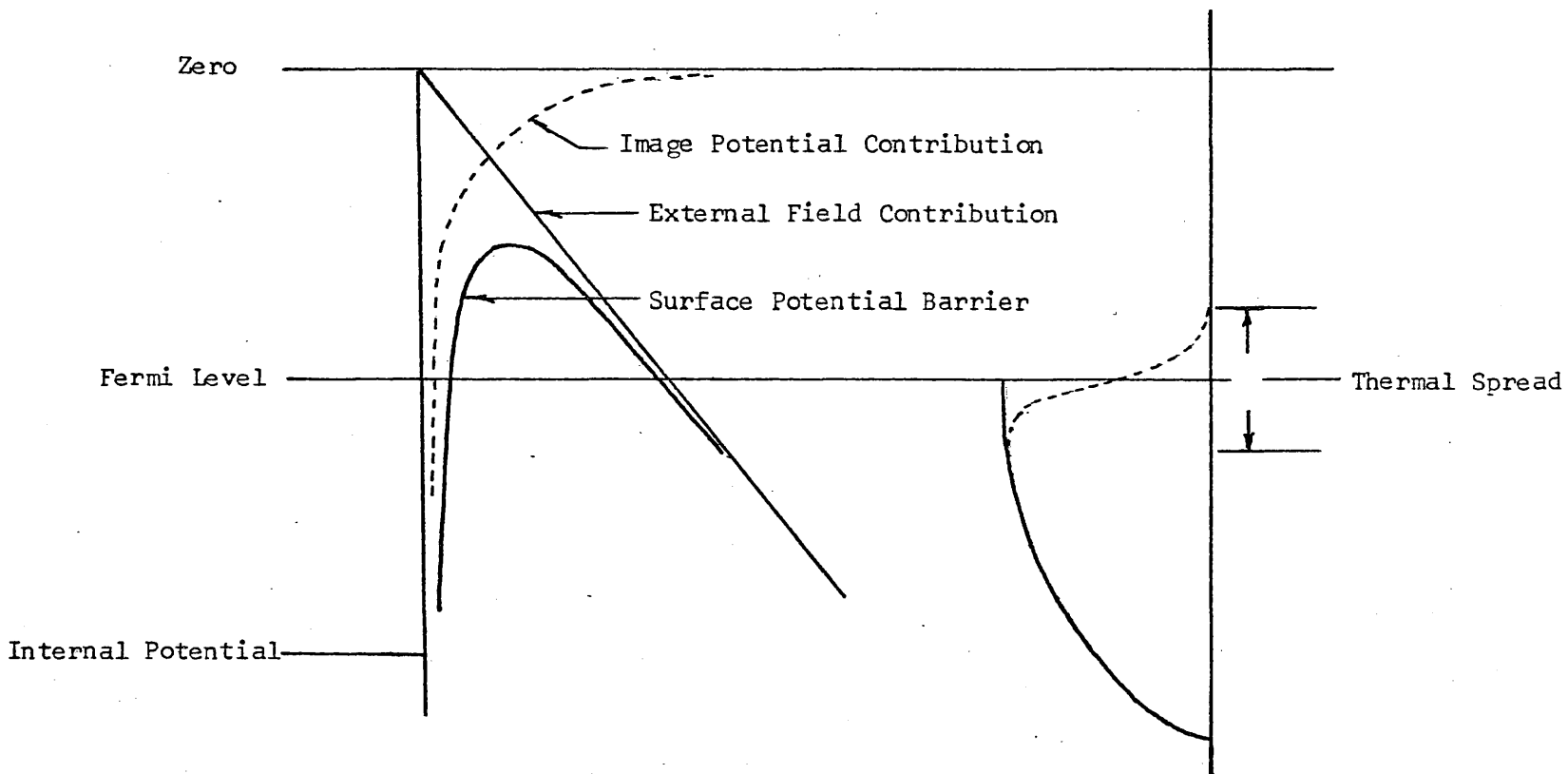


Fig. 1(A). Surface Potential Barrier

Appendix B

Heating of the Field Emitter During Operation

Consider the temperature rise of a field emitter, one end of which is kept at a low temperature by means of a liquid helium bath, when field emission current is drawn. We wish to calculate the maximum (worst case) steady state temperature as a function of the field emission current density and the geometry of the emitter. For this calculation, it is assumed that the only mechanism of heat loss (cooling) is by conduction through the end immersed in the helium reservoir. Two mechanisms of heat gain are considered: (1) Joule heating, and (2) heating due to the loss of electrons near the Fermi surface during emission.

The heat conduction equation is

$$\dot{Q} = - \int K \vec{\nabla} T \cdot d\vec{S} \quad [B.1]$$

where K is the thermal conductivity, T is the temperature, and dS a surface element. Making use of the divergence theorem, the heat conduction equation can be expressed in the form

$$\dot{Q} = - \int K (\vec{\nabla} \cdot \vec{\nabla} T) dV \quad [B.2]$$

Consider \dot{Q} , the left-hand-side of [B.2]. The specific heat of a substance is defined in the limit by

$$c = \lim_{T \rightarrow 0} (1/m) \Delta Q / \Delta T = (1/m) dQ/dT \quad [B.3]$$

Using [B.3], \dot{Q} can be expressed in terms of a temperature change per unit time

$$\dot{Q} = mc(dT/dt) \quad [B.4]$$

If m , the mass of the sample, is expressed in terms of its density, ρ then [B.4] can be rewritten in terms of an integral over a volume

$$\dot{Q} = \int_V c \rho (dT/dt) dV \quad [B.5]$$

Finally, adding a Joule source of heat, [B.2] takes the form

$$\int_V K (\vec{\nabla} \cdot \vec{\nabla} T) dV - \int_V c \rho (dT/dt) dV = - \int_V \vec{J} \cdot \vec{E} dV$$

which can be expressed in differential form

$$\nabla^2 T - (c \rho / K) (\partial T / \partial t) = -(1/K) \vec{J} \cdot \vec{E} \quad [B.6]$$

where \vec{J} is the current density and \vec{E} the electric field vector.

Since we are interested in the steady state solution only, we will ignore the term in time (t), so that the final equation which must be solved with appropriate boundary conditions is the following

$$\nabla^2 T = -(1/K) \vec{J} \cdot \vec{E} \quad [B.7]$$

If \vec{E} is written in terms of the electrical conductivity, σ , and current density \vec{J} , [B.7] is reduced to the form desired.

$$\nabla^2 T = -(1/K \sigma) J^2 \quad [B.8]$$

It will be assumed that the geometry of the field emitter can be

approximated by a cone, truncated at two points by concentric spheres which cut the emitter axis on the perpendicular (Fig. 1(B)). This model has been successfully used by Dolan, et al.¹² to predict the temperature rise of a field emitter during pulsed operation. Then, rewriting [B.8] in terms of r , the distance from the apex of the cone, and θ the cone half angle, we obtain the following differential equation

$$r^2 \partial / \partial r (r^2 \partial T / \partial r) = -(1/K\sigma)(I^2/4\pi^2(1-\cos \theta)^2) \quad [B.9]$$

where J has been written in terms of the total field emission current, I , and the area of a cut through the cone by a spherical surface. Carrying out the differentiation indicated in [B.9],

$$r^4 \partial^2 T / \partial r^2 + 2r^3 \partial T / \partial r = -I^2/4\pi^2 K\sigma (1-\cos \theta)^2 = b \quad [B.10]$$

the general solution of [B.10] is

$$T(r,I) = br^{-2}/2 + c_1 r^{-1} + c_2 \quad [B.11]$$

The arbitrary constants, c_1 and c_2 , are evaluated by imposing boundary conditions as follow: (1) at $r = l$, the temperature of the emitter is taken to be that of the bath temperature, usually 4.2°K in the experiments reported in this thesis, and (2) at some other point closer to the apex of the emitter, $r = u$, where the current density is a maximum, it will be assumed that heat is being introduced by the emission process and thus

$$(A(r) K \partial T / \partial r)_{r=u} = -I \Delta V$$

where ΔV is the difference between the average energy in the emitted current and the top of the Fermi distribution. Using these boundary conditions, the following values are found for c_1 and c_2

$$\begin{aligned} c_1 &= [I \Delta V / 2 \pi K (1 - \cos \theta)] - b/u \\ c_2 &= 4.2 - b/2l^2 + b/ul - (I \Delta V / 2 \pi K (1 - \cos \theta)) [1/l] \end{aligned}$$

Making these substitutions in [B.11]

$$\begin{aligned} T(r, I) &= 4.2 + b/2(r^{-2} - l^{-2}) + b/u(l^{-1} - r^{-1}) \\ &\quad + (I \Delta V / 2 \pi K (1 - \cos \theta))(r^{-1} - l^{-1}) \end{aligned} \quad [B.12]$$

Assuming $l \gg r$ and u , we can reduce [B.12] to

$$T(r, I) = 4.2 + 0.5r^{-2} - br^{-1}u^{-1} + [I \Delta V / 2 \pi K (1 - \cos \theta)]r^{-1} \quad [B.13]$$

If the maximum heating occurs at $r = u$, where the current density, J , is largest, then $T(u, I)$ at $r = u$, can be found from [B.13]

$$T(u, I) = 4.2 - 0.5bu^{-2} + [I \Delta V / 2 \pi K (1 - \cos \theta)]u^{-1} \quad [B.14]$$

Making the appropriate substitution for "b" from [B.10], $T(u, I)$ is expressed in terms of the current density, J , at $r = u$ and the energy distribution of the emitted current.

$$T(u, J) = 4.2 + 0.5(u^2 / \sigma K) J_u^2 + (u \Delta V / K) J_u \quad [B.15]$$

If u is taken to be $3r_0$, where $r_0 = 2 \times 10^{-5}$ cm is the radius of a typical field emitter, for values of I (10^{-8} amperes) used in this work, the current density at u is on the order of 30 A/cm^2 for $\theta = 10^\circ$.

The values of σ and K will vary with temperature and crystalline perfection. ΔV will vary with electric field strength, being smaller for weaker electric fields. A reasonable estimate would put $\Delta V \sim 1$ eV. White³⁵ suggests that K varies from one to 10 watts $\text{cm}^{-1} \text{deg}^{-1}$ at 4.2°K, depending on the perfection of the sample. $\rho(H)$, the magnetoresistance of bismuth, is on the order of 1 ohm-cm for the magnetic field strength of interest here. Letting $K = 1$ watt $\text{cm}^{-1} \text{deg}^{-1}$ and $\sigma = 1 \text{ ohm}^{-1} \text{cm}^{-1}$, the second and third terms in [B.15] become $1.62 \times 10^{-6} \text{°K}$ and $1.8 \times 10^{-4} \text{°K}$, respectively. Thus, it must be concluded that heating of the field emitter during operation by charge flow is insignificant in this work and can be ignored as a contribution to the diminishment of the amplitude of dHvA oscillations.

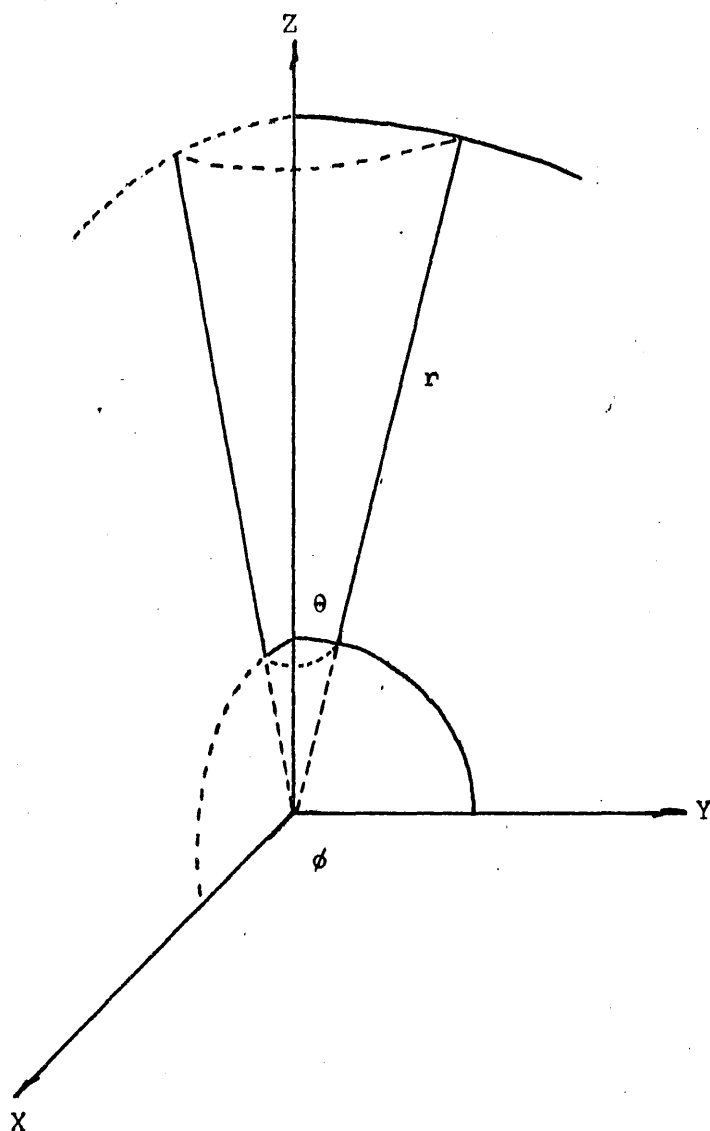


Fig. 1(B). Emitter Model

Appendix C

Size Effects

Size effects occur when the dimensions of the sample under investigation become small enough to interfere with quantized carrier orbits in the solid. Since the radius of a field emitter is usually on the order of a few thousand angstroms, it is desirable to calculate the real-space radii of quantized carrier orbits for bismuth.

The wave vector, \vec{k} , has a time derivative

$$\frac{d\vec{k}}{dt} = (e/\hbar c)(\vec{v} \times \vec{B}) \quad [C.1]$$

where \vec{B} is the magnetic flux density, \hbar is Planck's constant divided by 2π , and \vec{v} is the velocity of a carrier. Since the force on a carrier is always normal to its velocity, the carrier's energy is constant and it travels on an orbit in real space which has the same shape as the k-space orbit, but is rotated by 90° . When [C.1] is integrated and written in coordinate form for $\vec{B} = \hat{k}B_z$ (\hat{k} is a unit vector)

$$|r_x| = (hc/eB_z) |k_y| \quad [C.2]$$

The Fermi surface of bismuth has been reported by several authors to consist of a single hole ellipsoid which is oriented along the trigonal axis, and three equivalent electron ellipsoids, one principal axis and the other two tilted about 6° from the trigonal and bisectrix

axes. ^{2,22}

The dHvA periods for the electron ellipsoid are given in Table 1(C) below.

Table 1(C). dHvA Periods for Electrons and Holes in Bismuth ^{††}

Axes	Electrons		Holes	
	Periods (G ⁻¹)	Area (cm ⁻²)	Periods (G ⁻¹)	Area (cm ⁻²)
1	0.53x10 ⁻⁵	18.0x10 ¹²	0.45x10 ⁻⁵	21.2x10 ¹²
2	8.35x10 ⁻⁵	1.1x10 ¹²	0.45x10 ⁻⁵	21.2x10 ¹²
3	0.69x10 ⁻⁵	13.7x10 ¹²	1.58x10 ⁻⁵	6.1x10 ¹²

*R. N. Bhargava, Phys. Rev. 156, 785(1967).

[†]Periods and areas are in the ellipsoidal axes.

The extremal cross sectional area of an ellipsoid in the plane normal to the direction of \vec{B} is given by

$$A_{\text{ext}} = (2\pi e/\hbar c)(1/P) \quad [\text{C.3}]$$

where P is the period of the dHvA oscillations measured in reciprocal gauss (G⁻¹). Since the area of an ellipse in k-space can be expressed by

$$\pi k_x k_y = A_z$$

the values for the $|k_i|$ can be obtained from the known dHvA periods listed in Table 1(C). When this arithmetic is carried out, the

following values are obtained for the $|k_i|$ of electrons in the ellipsoidal axes:

$$k_1 = 5.17 \times 10^5 \text{ cm}^{-1} \quad [\text{C.4a}]$$

$$k_2 = 6.77 \times 10^5 \text{ cm}^{-1} \quad [\text{C.4b}]$$

$$k_3 = 8.46 \times 10^6 \text{ cm}^{-1} \quad [\text{C.4c}]$$

For the single hole ellipsoid, we obtain k values

$$k_1 = 1.39 \times 10^6 \text{ cm}^{-1} \quad [\text{C.5a}]$$

$$k_2 = 1.39 \times 10^6 \text{ cm}^{-1} \quad [\text{C.5b}]$$

$$k_3 = 4.86 \times 10^6 \text{ cm}^{-1} \quad [\text{C.5c}]$$

Using [C.2], the real space maximum radii can be calculated. For fields of 1 kG and 10 kG along the long axis of an electron ellipsoid (approximately bisectrix crystal axis), and normal to the long axis (binary crystal axis), we find real-space maximum radii

$$\text{(Electrons) } B \parallel \text{ bisectrix: } r = 4500\text{\AA}; \quad 1 \text{ kG} \quad [\text{C.6a}]$$

$$= 450\text{\AA}; \quad 10 \text{ kG}$$

$$B \parallel \text{ binary: } r = 56000\text{\AA}; \quad 1 \text{ kG} \quad [\text{C.6b}]$$

$$= 5600\text{\AA}; \quad 10 \text{ kG}$$

For hole orbits with B normal to the trigonal axis, or parallel to the trigonal axis, we find maximum radii

$$\text{(Holes) } B \perp \text{ trigonal: } r = 32200\text{\AA}; \quad 1 \text{ kG} \quad [\text{C.7a}]$$

$$= 3220\text{\AA}; \quad 10 \text{ kG}$$

(Holes) $B \parallel$ trigonal: $r = 9200\text{\AA}; 1 \text{ kG}$ [C.7b]
 $= 920\text{\AA}; 10 \text{ kG}$

It is evident that, for a field emitter of normal dimensions, size effects will be important for fields of less than 10 kG along a binary axis. At higher fields, however, size effects would probably not present a serious problem.